Representation of the direct correlation function of the hard-sphere fluid

S. Pieprzyk[*] and A. C. Brańka[†]
Institute of Molecular Physics, Polish Academy of Sciences, M. Smoluchowskiego 17, 60-179 Poznań, Poland

D. M. Heyes[‡]
Department of Physics, Royal Holloway, University of London, Egham, Surrey, TW20 0EX, United Kingdom
(Received 3 April 2017; published 2 June 2017)

An accurate representation of the structural pair correlation functions of the hard sphere (HS) fluid up to the freezing density is proposed which combines the pole expression for the total correlation function $h(r)$, the Ornstein-Zernike equation, and molecular dynamics (MD) computer simulation data. In the scheme, $h(r)$ is expressed in terms of a set of pole parameters, which reveals how the tail of the Fourier transform of $h(r)$ contains information on the discontinuities in the derivatives of the direct correlation function (DCF). This formulation leads to a DCF expressed as the sum of a numerically obtainable part and an analytic part which consists of elementary integral terms, some of which are found to give rise to the discontinuities. An exact formula for the magnitude of these discontinuities is derived, which indicates that there is a particular density ($\rho \cong 0.133$) below which the magnitude of the discontinuities decreases with increasing order of the derivative. With the accurate MD simulation data the set of parameters that specifies $h(r)$ was determined. These can be used to obtain the different structural functions of the HS fluid, and following the calculation stages of the pole structure scheme the DCF is obtained. From this route to the DCF the second pole of the HS fluid can be determined and the non-negligible role of the "out of core" part of the DCF at high densities is revealed. The density-dependent separation range where the two pole approximation represents well the $h(r)$ has been determined.

DOI: 10.1103/PhysRevE.95.062104

I. INTRODUCTION

Among the various properties of the liquid phase, the class of pair molecule structural correlation functions (SCFs) are of particular importance. The basic structural characterization of a simple homogeneous liquid is given by the radial distribution function (RDF) or $g(r)$, where r is the interparticle separation. This function can be obtained from the static structure factor from x-ray and neutron scattering experiments [1,2]. The RDF plays a fundamental role in statistical mechanical theories of liquids and, assuming the interactions between the molecules are pairwise additive, a wide range of thermodynamic properties can be expressed in terms of $g(r)$ [3], knowledge of which therefore leads to their calculation. Also, this function is a useful means of describing short-range order in amorphous solids [4–6].

In view of its fundamental importance it is no surprise that $g(r)$ has been the subject of numerous investigations for many years. The primary practical theoretical methods used to obtain the SCF are computer simulation and the integral equation liquid state theories based on the Ornstein-Zernike (OZ) relation [7],

$$h(r_{12}) = c(r_{12}) + \rho \int h(r_{13})c(r_{23})\, d\mathbf{r}_3, \qquad (1)$$

where ρ is the number density, $c(r)$ is the direct correlation function (DCF), and $h(r) = g(r) - 1$ is the total correlation function. The subscripts, 1,2,3 denote the positions of three molecules, where the separation between particles, i and j is $r_{ij} = \mid \mathbf{r}_i - \mathbf{r}_j \mid$. The DCF is the second derivative of the intrinsic free energy functional with respect to ρ [7], but is often defined through its inclusion in Eq. (1). The DCF represents that part of $h(r)$ which results from the direct correlation between particles, 1 and 2, and is connected with the isothermal compressibility via the exact relation, $\kappa = 1 - \rho \int d\mathbf{r} c(r)$. There are other SCFs that can be expressed in terms of the $h(r)$ and $c(r)$ functions which have also attracted interest. These include the indirect correlation function, $s(r) = h(r) - c(r)$, the bridge function, $b(r) = \ln[h(r) + 1] + \phi(r) - h(r) + c(r)$, and the cavity distribution function, $y(r) = \exp[h(r) - c(r) + b(r)]$. The $\phi(r)$ here is the interaction pair potential between particles in the fluid expressed in units of $k_B T$, where T is the temperature and k_B is Boltzmann's constant.

It is noteworthy that the basic functions, $g(r)$ and $c(r)$, are still only approximately known even for the simplest of model particles. Computer simulation, usually Monte Carlo (MC) or molecular dynamics (MD), gives numerical values for $g(r)$ within a finite radius r_c, but in practice the data generated are always within a certain level of precision, and the long-range behavior or "tail" where $r > r_c$, is not accessible directly from the simulation, which means, for example, that the small wave vector region ($q \to 0$) cannot be obtained without further approximation and assumptions. The integral equation liquid state theories can provide information on the tail but yield $g(r)$ at a more approximate level because solution of the OZ equation is subject to an imposed closure relation which can only ever be an approximation [7]. Even in this case, some aspects of the SCF remain incomplete even in the case of such a basic system as the hard sphere (HS) fluid.

The HS fluid constitutes one of the most fundamental examples of a model many-body system. The HS interaction mimics the extremely strong repulsion that atoms experience

[*]slawomir.pieprzyk@ifmpan.poznan.pl
[†]branka@ifmpan.poznan.pl
[‡]david.heyes@rhul.ac.uk

at close distance and is defined as the potential between two impenetrable spheres that cannot overlap i.e., $\phi(r < \sigma) = \infty, \phi(r > \sigma) = 0$, where σ is the HS diameter. Distance in this work is expressed in units of σ, and it is set equal to 1. The HS potential is the most basic representation of particles with excluded volume interactions, and as such has been used widely as the basis of theoretical studies of the physical properties and equation of state of a wide range of systems such as simple liquids, glasses, colloidal particles, and granular materials [8,9]. The HS model has been the foundation of many statistical mechanical models of the liquid state.

In this work we propose a framework which allows us to obtain an accurate representation of the SCF of the HS fluid. The approach combines the residue theorem analysis, accurate simulation data, and the OZ equation. Our aim is to obtain a more comprehensive representation and bring to light some new features of the HS fluid SCF. In the scheme adopted the contribution from the tail part is considered without any approximate closures, and its key role in providing an accurate description of the SCF is established. The focus here is on the DCF, which is considered to be the most inaccessible example of the different SCFs, and has perhaps surprisingly been the subject of relatively few investigations as a property in its own right. This situation may have arisen because the analytical formula for it from the Percus-Yevick approximation (PY), $c_{PY}(r)$ [10–13], has been available for many decades and is widely considered to be one of the most important results in the history of statistical mechanical liquid state theory. Also, some approximate analytical formulas for $c(r)$ have been proposed, mainly to overcome limitations of the PY theory. Tejero and López de Haro [14] derived analytic approximations for $c(r)$ based on a generalization of the PY result using the Rational Function Approximation, which circumvents the thermodynamic consistency problem [15,16]. Fukudome obtained improvements on the PY result for $c(r)$ derived from an extended version of scaled particle theory [17]. A powerful framework for determining the DCF is classical density functional theory. In particular, Rosenfeld's fundamental measure theory [18] and the White Bear II version of it provides accurate results for the DCF [19,20].

There have been several attempts to extract the HS $c(r)$ directly from the OZ equation using simulation data, often supplemented by extra parametrization of some parts of $g(r)$ or $c(r)$. The results obtained in this way by Groot *et al.* with MC [21] can be considered to be the first that showed convincingly the nontrivial behavior of $c(r)$ over a broad range of densities and r. These results were used by others to represent the HS $c(r)$ to test new methods and approximations of various liquid theories [14,22,23].

There have been a number of significant developments in the use of the HS $c(r)$. A method based on a pole analysis of the OZ equation has been developed [24–27] to study the decay of the pair correlation functions in simple liquids. It was shown by using the residue theorem of complex analysis how a pole structure determines the asymptotic behavior of $g(r)$. In particular, the method enables the crossover from monotonic to damped oscillatory decay or the so-called Fisher-Widom (FW) line [28] to be determined. The asymptotic decay of several model fluids (and their mixtures), e.g., the Lennard-Jones, HS [23,27], and Yukawa liquids [29], has been made using the pole approach. Also, it has been used to investigate the decay of structural correlations in the one-component plasma [30] and inverse power fluid [31]. Basically, the scheme requires $c(r)$ as input, and usually studies of the asymptotic decay have employed its approximate representation. In the case of the HS fluid the PY approximation was considered the most suitable one, and the pole structure in this approximation has been the subject of several studies [32–34]. The first study of the asymptotic decay exploiting simulation data was performed by Dijkstra and Evans [23]. The numerical procedure was restricted to the calculation of the two leading poles, and it was shown that the two-pole formula based on the leading complex and purely imaginary poles captures well the FW line. In this work the pole scheme is used to go beyond the asymptotic analysis and treat formally the RDF of the HS fluid as represented by a set of poles.

Extensive studies determining the bridge function of HSs have been performed using accurate simulation data and the OZ equation [35,36]. The calculated $b(r > 1; \rho)$, for a number of densities within the whole fluid range (including the metastable region) up to $\rho = 1.02$ are available numerically and as functional fits [36]. From those studies the DCF for the distance range $r > 1$ can be estimated. At low densities, the SCF can be expressed as an expansion in density, where it is feasible to calculate the expansion coefficients and functions by diagrammatic techniques. An expansion of the bridge and radial distribution function up to the sixth order in density was obtained by Kolafa and Labík [37]. The presence of discontinuities in the higher derivatives of the corresponding expansion functions and coefficients [i.e., $E_n(r)$ and $H_n(r)$] were discussed. In particular, it was shown that the finite distance (r) range of the expansion functions caused a "jump" or discontinuity in their $(2k-2)$-th derivative at $r = k$, where $k = 1,2,\ldots$. This work is organized as follows. In Sec. II the theory of the radial and direct distribution functions is covered, focusing especially on the small and large wave vector limits. In Sec. III MD computer simulation results are used to compute these distribution functions. A summary of the main conclusions of this work is given in Sec. IV.

II. THEORY

From the general properties of the $c(r)$ and $h(r)$ functions it follows that for a wave vector q in the complex plane [24] the following formula applies:

$$h(r) = \frac{1}{4\pi^2 \mathrm{i}r} \int_{-\infty}^{+\infty} dq q e^{\mathrm{i}qr} \frac{c(q)}{1-\rho c(q)}, \tag{2}$$

where $c(q)$ denotes the Fourier transform of $c(r)$. Any poles at $q = \omega + \mathrm{i}\alpha$ are given by the zeros of the denominator, $1 - \rho c(q) = 0$, and from this equation, by equating real and imaginary parts, the formulas [25]

$$4\pi\rho \int_0^\infty dr r^2 c(r) \frac{\sinh(\alpha r)}{\alpha r} \cos(\omega r) = 1, \tag{3}$$

$$4\pi\rho \int_0^\infty dr r^2 c(r) \cosh(\alpha r) \frac{\sin(\omega r)}{\omega r} = 1, \tag{4}$$

are obtained. If $c(r)$ is known and decays sufficiently rapidly, the above equations provide a practical route to obtain the poles [23,25,26]. The integral in Eq. (2) can be evaluated using the residue theorem to give

$$h(r) = \sum_{i=1}^{\infty} \frac{R_i}{r} e^{\mathrm{i}q_i r}, \tag{5}$$

where $q_i = \omega_i + \mathrm{i}\alpha_i$ is the ith pole, and R_i is the residue at $q = q_i$. In the case of the HS model the complex poles occur only in conjugate pairs, so after summing conjugated poles,

$$h(r) = \sum_{i=1}^{\infty} \frac{2\mathcal{A}_i}{r} e^{-\alpha_i r} \sin(\omega_i r + \delta_i), \tag{6}$$

is obtained, where $\mathcal{A}_i$ and δ_i are the amplitude and phase, which can be calculated according to the formulas derived in Refs. [23,25]. It follows directly from Eq. (6) that the rate of decay of $h(r)$ is determined by the exponential terms, so at large r the dominant contribution comes only from terms with the smallest α. Thus, to determine the asymptotic behavior of the radial distribution function it is sufficient to calculate [e.g., with Eqs. (3)–(4)] the leading pole, i.e., the one which is closest to the real axis. For a given ρ, the set $\{\mathcal{A}_1,\alpha_1,\omega_1,\delta_1,\mathcal{A}_2,\alpha_2,\omega_2,\delta_2,\ldots\} \equiv \{\mathcal{X}\}$ completely represents the $h(r)$ and from the nature of the HS interaction it follows that for any $r < 1$ the series must sum up to -1. So the final representation of $h(r)$ of the HS fluid in terms of the pole structure or $\{\mathcal{X}\}$ is

$$h(r) = \begin{cases} -1 & \text{for r} < 1, \\ \sum_{i=1}^{\infty} \frac{A_i}{r} e^{-\alpha_i r} \sin(\omega_i r + \delta_i) & \text{for r} > 1, \end{cases} \tag{7}$$

where now A_i is used for $2\mathcal{A}_i$. It is noteworthy that the Fourier transform of the above representation for $h(r)$ is given by the analytic expression

$$\begin{aligned} h(q) = &-\frac{4\pi}{q^2}\left[\frac{\sin(q)}{q} - \cos(q)\right] + \frac{2\pi}{q}\sum_{i=1}^{\infty} A_i e^{-\alpha_i} \\ &\times \left[\frac{\alpha_i \cos(\delta_i + \omega_i - q) - (\omega_i - q)\sin(\delta_i + \omega_i - q)}{\alpha_i^2 + (\omega_i - q)^2}\right. \\ &\left. - \frac{\alpha_i \cos(\delta_i + \omega_i + q) - (\omega_i + q)\sin(\delta_i + \omega_i + q)}{\alpha_i^2 + (\omega_i + q)^2}\right]. \end{aligned} \tag{8}$$

A. Large q-limit

Next it is important to note that the large q-limit or tail of the above $h(q)$ [Eq. (8)] can be expressed (see Appendix A) in the relatively simple form

$$h_{\text{tail}}(q) = \cos(q)\left[\sum_{n=1}^{\infty} \frac{C_n}{q^{2n}}\right] + \sin(q)\left[\sum_{m=1}^{\infty} \frac{D_m}{q^{2m+1}}\right]. \tag{9}$$

The C_n and D_m coefficients depend on the $\{\mathcal{X}\}$ set, and the few first coefficients are given in Appendix A. It is also shown in Appendix A that these coefficients are related and can be expressed in terms of derivatives of the RDF at contact (i.e., at $r = 1$), where

$$C_1 = \frac{6Z}{\rho}, \quad D_1 = -4\pi\left[g(r) + \frac{dg(r)}{dr}\right]_{r=1}, \tag{10}$$

$$C_2 = -4\pi\left[2\frac{dg(r)}{dr} + \frac{d^2g(r)}{dr^2}\right]_{r=1},$$

$$D_2 = -4\pi\left[3\frac{d^2g(r)}{dr^2} + \frac{d^3g(r)}{dr^3}\right]_{r=1}, \tag{11}$$

and $Z = P/\rho k_B T - 1$, P is the pressure. Thus, as seen from Eqs. (10)–(11), the tail of the structure factor, $S(q) = 1 + \rho h(q)$ contains considerable information about $g(r)$ at contact.

Taking into account the OZ relation and that for large wave vectors $\rho h(q) < 1$, the expression, $c_{\text{tail}}(q) = h_{\text{tail}}(q)/[1 + \rho h_{\text{tail}}(q)] = \sum_{k=1}^{\infty}(-\rho)^{k-1} h_{\text{tail}}^k(q)$, can be derived. Exploiting the binomial formula, $(a+b)^k = \sum_{s=0}^{k} \binom{k}{s} a^{k-s} b^s$ for the $h_{\text{tail}}^k(q)$, the following formula for $c_{\text{tail}}(q)$ is obtained:

$$\begin{aligned} c_{\text{tail}}(q) = &\sum_{k=1}^{\infty}(-\rho)^{k-1}\sum_{s=0}^{k}\binom{k}{s}\cos(q)^{k-s} \\ &\times \sin(q)^s\left[\sum_{n=1}^{\infty}\frac{C_n}{q^{2n}}\right]^{k-s}\left[\sum_{m=1}^{\infty}\frac{D_m}{q^{2m+1}}\right]^s. \end{aligned} \tag{12}$$

Finally, the part of the DCF produced by the tail of $c(q)$ is

$$\begin{aligned} c_A(r) &= \frac{1}{2\pi^2}\int_Q^{\infty} dq q^2 c_{\text{tail}}(q)\frac{\sin(qr)}{qr} \\ &= \frac{1}{2\pi^2 r}\sum_{k=1}^{\infty}(-\rho)^{k-1}\sum_{s=0}^{k}\binom{k}{s}\int_Q^{\infty} dq q \sin(qr) \\ &\quad \times \cos(q)^{k-s}\sin(q)^s\left[\sum_{n=1}^{\infty}\frac{C_n}{q^{2n}}\right]^{k-s}\left[\sum_{m=1}^{\infty}\frac{D_m}{q^{2m+1}}\right]^s, \end{aligned} \tag{13}$$

where Q denotes an arbitrarily large wave vector. The DCF is thus considered to be a sum of two components, $c(r) = c_N(r) + c_A(r)$, the analytically derived $c_A(r)$ part in Eq. (13), and a numerically obtainable term,

$$c_N(r) = \frac{1}{2\pi^2}\int_0^{Q} dq q^2 \frac{h(q)}{1 + \rho h(q)}\frac{\sin(qr)}{qr}, \tag{14}$$

with $h(q)$ given in Eq. (8). Both $c_A(r)$ and $c_N(r)$ display oscillations which are particularly noticeable near $r = 0$ and $r = 1$. This effect is seen in Fig. 1, where an example of the DCF, and its $c_A(r)$ and $c_N(r)$ parts are plotted near $r = 1$ for two different Q values. Their relative contributions to $c(r)$ as well as their form is regulated by the Q value, but the sum is Q independent, at least for some sufficiently large Q value (see the bold line in Fig. 1). Therefore, $c_A(r)$, and consequently the function, $c_{\text{tail}}(q)$ [or equivalently $h_{\text{tail}}(q)$] contain important and necessary information which cannot be omitted in any accurate representation of $c(r)$.

In principle, the complete pole structure $\{\mathcal{X}\}$ would be required to determine $c_A(r)$ and $c_N(r)$ completely. Although it is expected that for distances $r > 1$, the series involved in the expressions will converge sufficiently rapidly that a

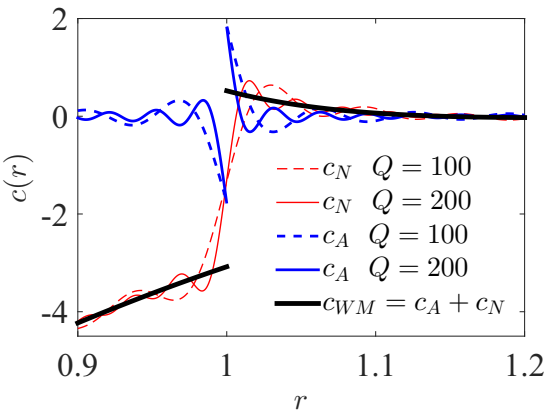

FIG. 1. The DCF (bold solid line) near the discontinuity at $r = 1$, expressed as a sum of the analytically derived part $c_A(r)$ [see Eq. (13)] and numerically obtained part $c_N(r)$ [see Eq. (14)] and determined according to the scheme in Sec. III. Examples for two different Q values are shown, denoted by solid and dashed thin lines. The HS density is $\rho = 0.75$.

summation over all the terms is not required for an accurate result. This issue is treated further in Sec. III. The expression in Eq. (13) for $c_A(r)$ reveals some general features of the DCF. As may be seen, $c_A(r)$ is composed of terms with integrals of the type $\int_Q^\infty dq\, \sin(qr)\cos(q)^{k-s}\sin(q)^s/q^L$, where L is a positive integer. The infinite number of such integrals may be grouped into three categories, (a) integrals with $s = 0$, (b) integrals with $s = k$, and (c) all the remaining ones ($s \neq k$, $s \neq 0$). They are analyzed and discussed in Appendix B. The main result obtained in Appendix B is that the integrals that cause discontinuities in the DCF derivatives are identified.

It is shown in Appendix B that the discontinuities come from an integral term of the form, $I(r) = (r-a)^{L-1}\int_Q^\infty dq\, \sin[q(r-a)]/q^L$, where a and L are positive integers which emerge in the calculations of the terms with $s = 0$ or $\binom{k}{0}$ type of integrals. The reason for the presence of the discontinuities follows from the properties of the sine integral special function [38], which causes the integral $\int_Q^\infty dq\, \sin[q(r-a)]/q = \frac{\pi}{2}|\, r-a\,|/(r-a) - Si[Q(r-a)]$ where $Si(x) = \int_0^x dt\, \sin(t)/t$, to have a jump of π at $r = a$ and $I(r)$ to have a discontinuity in its $(L-1)$-th derivative.

Our detailed analysis of all types of integrals involved in Eq. (13) has shown that the leading discontinuities are generated by the $\binom{k}{0}$ integrals in which $L = 2k-1$, i.e., by terms of the form

$$\sum_{k=1}^{\infty}(-\rho)^{k-1}C_1^k\int_Q^\infty dq\,\frac{\sin(qr)\cos(q)^k}{q^{2k-1}}. \tag{15}$$

By the leading discontinuity we mean here a jump in the $(2k-2)$-th derivative at $r = k$, and that some other integrals generate a discontinuity at $r = k$ but in the higher than $(2k-2)$-th order derivatives of $c(r)$. This result, obtained with the pole structure approach, is significant because it demonstrates that discontinuities in the $(2k-2)$-th derivative at $r = k$ found for low densities by the diagrammatic method [37] are also present at any HS fluid density. Moreover, using Eq. (15), the magnitude of the jump in the leading discontinuities can be evaluated from

$$\triangle_k = \frac{(3Z)^k}{2\pi\rho k}, \tag{16}$$

which is an exact result that is not in the literature as far as we are aware. Thus, the second, fourth, and sixth derivatives have jumps of magnitude, $\triangle_2 = \frac{9Z^2}{4\pi\rho}$, $\triangle_3 = \frac{27Z^3}{6\pi\rho}$, and $\triangle_4 = \frac{81Z^4}{8\pi\rho}$ at $r = 2,3,4$, respectively. At $r = 1$ we have the well-known result $\triangle_1 = \frac{3Z}{2\pi\rho}$ in the $c(r)$ function, i.e., in its 0-order derivative. For $Z > 1/3$ the sequence of $\triangle_k$ increases and for $Z \leqslant 1/3$ decreases towards zero on increasing k. This indicates that in the HS fluid a particular density exists at $\rho_c = 0.1327$ (corresponding to the condition $Z = 1/3$ and Z from [36]) such that for $\rho < \rho_c$ the $c(r)$ becomes a smoother function. It would be interesting to relate ρ_c to a change in a physical quantity, but this appears not to be a simple task. In the limit $\rho \to 0$ all discontinuities tend to zero as $\triangle_k = (2\pi\rho)^{k-1}/k$, apart from $\triangle_1 \to 1$, which gives the correct ideal gas limit.

The analysis thus far shows that information about the $c(r)$ discontinuities is contained in the $c_{\text{tail}}(q)$ and cannot be convincingly inferred from the numerical part Eq. (14) for any finite Q value. Also we point out that in our analysis we were not able to find terms generating discontinuities at noninteger values of r, in particular at $r = \sqrt{3}$, which was reported by the diagrammatic approach to give a discontinuity in the low-density expansion [37].

B. Small q-limit

It can be shown that for small q the expression in Eq. (8) reduces to a polynomial in even powers of q, that is,

$$\lim_{q\to 0} h(q) = h^{(0)} + h^{(2)}q^2 + h^{(4)}q^4 + \cdots, \tag{17}$$

where

$$\begin{aligned} h^{(0)} = &-\frac{4\pi}{3} \\ &+ 4\pi\sum_{i=1}^{\infty}\frac{A_i e^{-\alpha_i}}{\left(\alpha_i^2+\omega_i^2\right)^2}\big[2\alpha_i\omega_i\cos(\delta_i+\omega_i) \\ &+ \alpha_i^2\omega_i\cos(\delta_i+\omega_i) + \omega_i^3\cos(\delta_i+\omega_i) \\ &+ \alpha_i^2\sin(\delta_i+\omega_i) + \alpha_i^3\sin(\delta_i+\omega_i) - \omega_i^2\sin(\delta_i+\omega_i) \\ &+ \alpha_i\omega_i^2\sin(\delta_i+\omega_i)\big]. \end{aligned} \tag{18}$$

The higher order coefficients are similar in form but are more cumbersome expressions. This first coefficient is also involved in the long-wave limit of the static structure factor, $S(0) = 1 + \rho h^{(0)}$, which can be obtained readily from an accurate HS equation of state, $Z = P/\rho k_B T - 1$, exploiting the exact relation, $S(0) = [\rho Z' + Z + 1]^{-1}$.

It can be confirmed that for small q, the function, $c(q) = h(q)/[1+\rho h(q)]$ is even in q, and

$$\lim_{q\to 0} c(q) = c^{(0)} + c^{(2)}q^2 + c^{(4)}q^4 + \cdots, \tag{19}$$

where the coefficients are functions of $\{\mathcal{X}\}$. The above expansion is a known feature of systems with a finite ranged

interparticle interaction, and the coefficients are given by [27]

$$c^{(2n)} = \frac{4\pi(-1)^n}{(2n+1)!}\int_0^\infty dr c(r) r^{2n+2}. \tag{20}$$

Thus, the $c^{(2n)}$ can be evaluated from the $c(r)$ function or from the corresponding set $\{\mathcal{X}\}$, which provides a demanding test of the accuracy and self-consistency of the DCF evaluation procedure adopted here.

III. DETERMINATION OF THE SCF

Both $h(r)$ and $c(r)$ are discontinuous functions at $r = 1$ and their exact representation by a series of continuous functions requires an infinite number of terms in Eq. (7) or equivalently the complete pole structure $\{\mathcal{X}\}$ needs to be included. For large r separations only a few terms (or poles) with the smallest α in Eq. (7) are required to obtain an accurate representation of $h(r)$. In general, for any specific separation, $R > 1$, there exists a finite number of terms, M, which provides an accurate result for $h(r > R)$. The value of M depends on R, density, and the required accuracy. For R close to unity, M becomes very large, and in the limit $R \to 1$ it tends to ∞.

For the above reasons, to obtain an accurate $c(r)$, the following analytic representation of $h(r)$ in the form of two functional parts is considered,

$$h_{WM}(r) = \begin{cases} -1 & \text{for } 0 < r < 1, \\ h_W(r) = \sum_{i=1}^{W} b_i r^i & \text{for } 1 < r < R, \\ h_M(r) = \sum_{i=1}^{M} \frac{A_i}{r} e^{-\alpha_i r}\sin(\omega_i r + \delta_i) & \text{for } r > R, \end{cases} \tag{21}$$

where now $\{b_1, b_2, \ldots, b_W\}$ and $\{A_1, \alpha_1, \omega_1, \delta_1, A_2, \alpha_2, \omega_2, \delta_2, \ldots, A_M, \alpha_M, \omega_M, \delta_M\}$ are parameters we denote by $\{\mathcal{X}_{WM}\}$. The form of $h_W(1 < r < R)$ is fairly arbitrary, but we seek a rather simple function, the Fourier transform of which can be obtained analytically. The polynomial form of $h_W(r)$ in Eq. (21) is convenient in this respect and provides sufficient flexibility in the next steps of the calculation. It is evident that the final results should be as insensitive as possible to the particular choice of W, R, and M values. Our tests suggest that a good compromise here, for most densities, is when W, M are in the range of approximately 10–15 and $R = r_{\min}$, where $r_{\min}$ is the position of the first minimum in the exact $h(r)$.

Different physical conditions can be imposed on $h_{WM}(r)$ and the following six have been applied in the scheme. These are the continuity and minimum conditions,

$$h_W(R) = h_{\min}, \quad h_M(R) = h_{\min}, \tag{22}$$

$$\left.\frac{\partial h_W(r)}{\partial r}\right|_R = 0, \quad \left.\frac{\partial h_M(r)}{\partial r}\right|_R = 0, \tag{23}$$

and the two thermodynamic relations,

$$Z = \frac{2\pi\rho}{3}(h_{WM}(1) + 1), \quad S(0) = [\rho Z' + Z + 1]^{-1} = 1 + 4\pi\rho\int_0^\infty r^2 h_{WM}(r)\, dr, \tag{24}$$

where $h_{\min} = h(R = r_{\min})$ and Z was taken from the very accurate HS equation of state proposed by Kolafa *et al.* [39]. The conditions in Eqs. (22)–(24) were used also by Trokhymchuk *et al.* [40] in their studies of the analytic expression for the RDF.

Equations (21)–(24) along with the scheme discussed in Sec. II can be used as a practical means of determining the SCF of the HS fluid. The main calculation stages are given in Appendix C. The set of parameters in Eq. (21) was determined based on the minimum condition for $|h_{WM}(r) - h_{MD}(r)| < 10^{-3}$ for each $r \in (1, r_c)$, where $h_{MD}(r)$ was obtained from the MD simulations. In the calculations a nonlinear fitting procedure was used, taking $r_c = 10$. We consider that the $h_{WM}(r)$ function obtained is an accurate representation of the exact $h(r)$ function. It has been shown [35,41] that the numerical data must be highly accurate to obtain reliable results for the bridge functions. In particular the data for $h_{MD}(r < r_c)$ must be obtained from long simulations with a large number of particles ($N > 10^4$). Only in this way can the effects of the finite size and the statistical errors in the simulations be reduced sufficiently. Because the calculations of $c(r)$ demand a similar level of accuracy as the bridge function we performed the simulations with a large system of $N = 16\,384$ HSs. Additionally, in order to test the N dependence or the finite size effects, some calculations were also carried out for systems of $N = 2916, 4000, 6912$, and 8788 particles, and it was confirmed that the simulations ought to be performed with large systems of $N > 10^4$. The calculations of $h_{MD}(r)$ were performed with the standard HS MD method [42] for a number of different densities representative of the entire fluid region, up to $\rho = 0.94$, which is near the freezing density. The histogram grid size was set to $\delta r = 0.01$ which was found to be optimal here. The MD simulations were carried out typically for a total number of 8×10^9 collisions, and the statistical uncertainty of the $h_{MD}(r)$ function was obtained with the block averaging method [43]. For each density and in the whole range of $r \in (1, r_c)$ the accuracy of $h_{MD}(r)$ is such that the estimated uncertainty was $< 10^{-3}$ and was up to 0.001 near contact for the highest densities and became less than 0.0001 at larger particle separations. For a large system the finite size effects for the MD calculations of the RDF arise mainly from fixing the particle number, i.e., from the relation between canonical and grand-canonical ensembles. The corrections required to convert data from the MD to the canonical ensemble are of $O(1/N^2)$, which are negligible here [44,45]. Thus, the calculated $h_{MD}(r)$ values were corrected using the leading order correction factor $[1 + S(0)/N]$. Also, it was checked for a few densities that the remaining part of the correction factor involving density derivatives was smaller than the obtained data accuracy and therefore could be neglected.

The resulting values of the parameters $\{\mathcal{X}_{WM}\}$ for $h_{WM}(r)$ are given in the tables in Supplemental Material [46]. The obtained parameters needed for Eq. (21) provide a highly accurate representation of the RDF of the HS fluid throughout the whole r-range, or $h(1 < r < \infty)$. Consequently, the $h_{WM}(r)$ function, which obeys several physical conditions [namely, Eqs. (22)–(24)], is readily accessible and can be made use of in more accurate statistical mechanical theories of the liquid state.

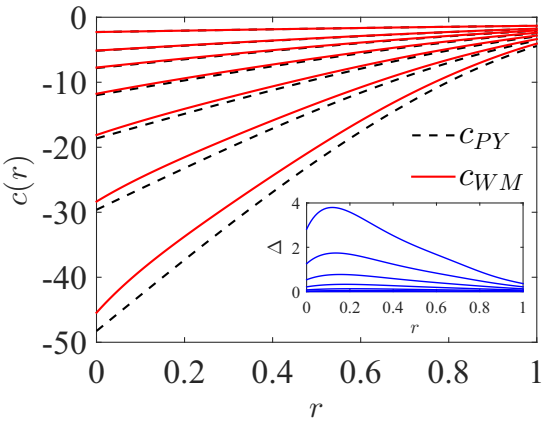

FIG. 2. The DCF for the $0 < r < 1$ region of pair separations, and for different densities. From top to bottom: $\rho = [0.2,0.4,0.5,0.6,0.7,0.8,0.9]$. The solid lines represent the DCF obtained from the WM representation of Eq. (21), and the dashed lines are from the PY approximation. In the inset the differences, $\Delta = c_{WM}(r) - c_{PY}(r)$ are shown (the largest discrepancy corresponds to the largest density). The density dependence of the limiting values is well represented by the polynomial function: $c_{WM}(r = 0; \rho) = -1 - 4.2026\rho - 8.2359\rho^2 - 6.6560\rho^3 - 53.401\rho^4 + 162.42\rho^5 - 361.47\rho^6 + 356.46\rho^7 - 158.92\rho^8$, and $c_{WM}(r = 1; \rho) = -1 - 1.3392\rho - 0.2956\rho^2 - 8.1336\rho^3 + 33.649\rho^4 - 83.532\rho^5 + 112.82\rho^6 - 79.862\rho^7 + 22.783\rho^8$.

Next, with the obtained $h_{WM}(r)$, the $c_{WM}(r)$ were determined according to the scheme presented in Sec. II and Appendix C. In the applied scheme, all the main sources of error [35,41] were minimized or eliminated. Specifically, the finite size and statistical errors were mitigated by using a large N, with long simulations and the appropriate correction factors. In the case of the tail errors these were minimized by the explicit incorporation of the tail terms, and for the grid-type errors, by reducing the numerical integration procedure to obtain $c_N(r)$ in the OZ equation to only one stage.

The obtained DCF is shown and discussed below, separately for $0 < r < 1$ (the inside-core part) and for $r > 1$. The DCFs are given in tables in Appendix D, which extend and improve on the $c(r)$ data of Groot *et al.* [21]. The results for $c(0 < r < 1)$ can conveniently be presented in the polynomial form:

$$c_{WM}(0 < r < 1; \rho) = \sum_{m=1}^{11} \lambda_m(\rho) r^{m-1}. \tag{25}$$

The coefficients λ_m are given in the first table in Appendix D, and the resulting DCF is shown for a few selected densities in Fig. 2 along with the PY result. As may be seen, the DCF is monotonically increasing in r and monotonically decreasing in ρ, and in general its character is similar to that of $c_{PY}(r)$. The inset shows that, apart from at low densities, the difference between them is substantial, however, and is most pronounced at separations near to 0.1, which might be connected with the absence of a quadratic term in the PY solution. The limiting values $c_{WM}(r = 0; \rho)$ and $c_{WM}(r = 1; \rho)$ are well represented by a polynomial function, which is given in the figure caption. They also can be

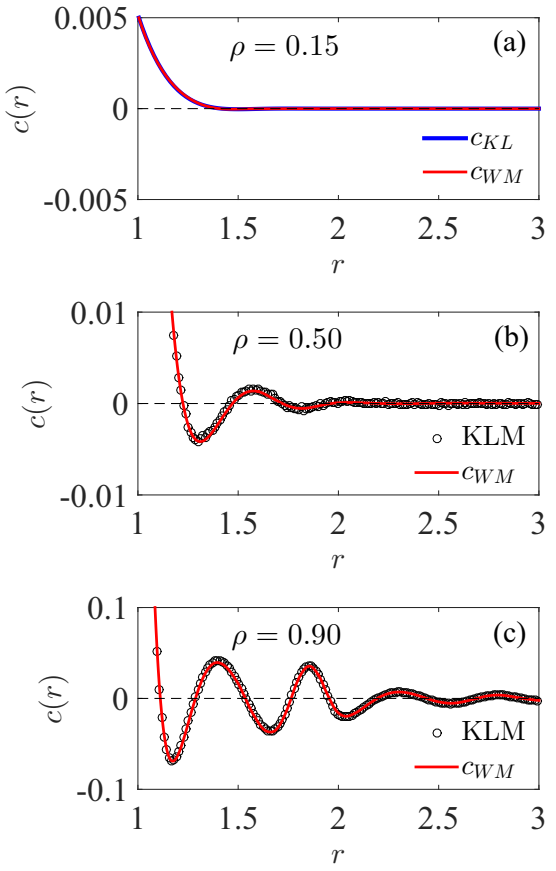

FIG. 3. The DCF, $c_{WM}(r)$, denoted as a (red) solid line for the $r > 1$ region and for (a) low, (b) intermediate, and (c) high density values, given on the figure. The thin (blue) line on frame (a) represents the DCF result of the low-density expansion approach (labeled c_{KL}) from Ref. [37], showing that the line overlies $c_{WM}(r)$. The open circles on frames (b) and (c) denoted as KLM are results obtained from the bridge functions calculated by Kolafa *et al.* [35,36].

expressed in terms of the corresponding PY solution values, $c_{WM}(0; \rho) \approx -1 + [1 + c_{PY}(0; \rho)]/(1 + 0.085\rho^{2.78})$ and $c_{WM}(1; \rho) \approx -1 + [1 + c_{PY}(1; \rho)]/(1 + 0.153\rho^{2.25})$. We emphasize that reliable and accurate results for these limiting functions cannot be obtained without the $c_A(r)$ part, as can be seen in Fig. 1.

The DCF for $r > 1$ is shown in Fig. 3 for several densities. As is known and clear in the figure, the DCF function decays very quickly in an oscillatory manner. It was checked that the available data for the bridge function [47] after converting to the DCF, $c(r) = b(r) + h(r) - \ln[1 + h(r)]$, are in excellent agreement with our results, and an example of such good agreement is shown in Fig. 3 for intermediate and high-density states (i.e., $\rho = 0.5$ and 0.9). For $\rho = 0.15$ [shown in Fig. 3(a)] a comparison is made with the DCF function $c_{KL}(r)$ obtained from the low-density expansion functions [37], and within the accuracy of 2×10^{-4} the results are indistinguishable. From our calculations for a range of low densities (0.05–0.20) it may be said that $c_{KL}(r)$ can represent the DCF for any $\rho < 0.15$. With the determined DCF the expansion coefficients in Eq. (19) can be calculated from the corresponding integrals in Eq. (20). The same coefficients can also be evaluated from

TABLE I. The expansion coefficients $c^{(2n)}$ in Eq. (19).

ρ	$c^{(0)}$	$c^{(2)}$	$c^{(4)}$
0.05	−4.6278	0.4577	−0.0164
0.10	−5.1283	0.5008	−0.0180
0.15	−5.7010	0.5486	−0.0193
0.20	−6.3583	0.6029	−0.0212
0.25	−7.1157	0.6646	−0.0231
0.30	−7.9920	0.7316	−0.0236
0.35	−9.0100	0.8154	−0.0282
0.40	−10.1983	0.9055	−0.0301
0.45	−11.5923	1.0119	−0.0333
0.50	−13.2363	1.1328	−0.0359
0.55	−15.1867	1.2738	−0.0382
0.60	−17.5152	1.4486	−0.0457
0.65	−20.3139	1.6535	−0.0535
0.70	−23.7021	1.8933	−0.0604
0.75	−27.8356	2.2218	−0.1010
0.80	−32.9204	2.5391	−0.0831
0.85	−39.2380	2.9608	−0.0911
0.88	−43.7864	3.3194	−0.1237
0.90	−47.2125	3.5344	−0.1252
0.92	−51.0198	3.8624	−0.1559
0.94	−55.2920	4.2377	−0.1925

their definition in terms of $\{\mathcal{X}_{WM}\}$ [note in this case $c(r)$ is not needed], and we checked that both approaches give practically the same values. Discrepancies are of order 10^{-3} at the highest densities considered, which demonstrates the accuracy and self-consistency of the pole structure scheme. The resulting $c^{(2n)}$ coefficients are given in Table I.

It is noteworthy that the predicted jump [see Eq. (16)] in the second derivative of the DCF at $r = 2$ is clearly visible in the $c_{WM}(r)$ determined, as shown in Fig. 4 for $\rho = 0.75$. As discussed in Sec. II (and Appendix B) and seen in the figure, the discontinuity comes from the $c_A(r)$ part determined from $h_{\text{tail}}(q)$. If that part is not included, even very accurate numerical data, such as the KLM data

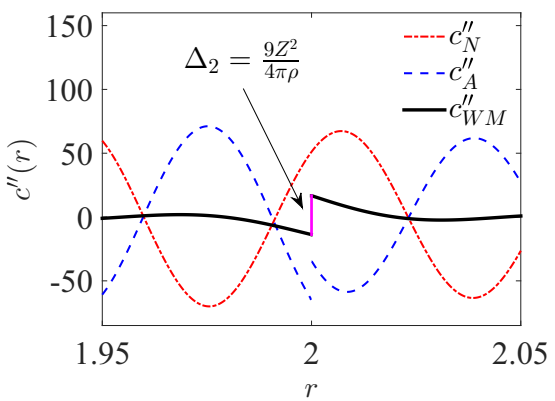

FIG. 4. Second derivative of the DCF near $r = 2$ for the density $\rho = 0.75$ (solid bold line). The second derivatives of the $c_A(r)$ and $c_N(r)$ parts are shown separately with thin dashed lines. The jump in the second derivative of DCF at $r = 2$ given from Eq. (16) is also indicated.

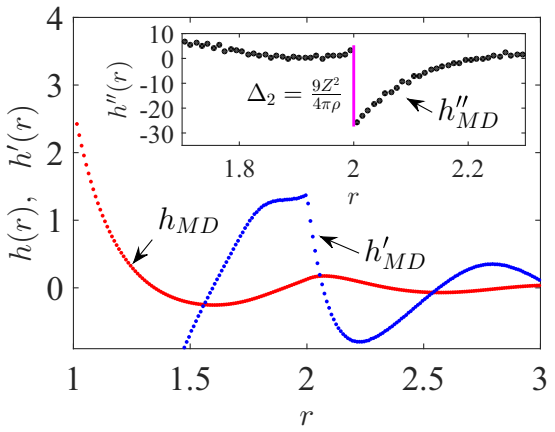

FIG. 5. The $h_{MD}(r)$ function (red dots) and its first derivative (blue dots) for the density, $\rho = 0.75$. In the inset the jump in Eq. (16) in the second derivative of the RDF is compared with the numerical result.

(the open circles in Fig. 3) in Fig. 4, can display the smooth second derivative of the DCF, $c''(r)$. In Fig. 5 the second derivative of $h_{MD}(r)$ demonstrates the presence of the same jump in the RDF function, a result which follows also from its low-density expansion [37]. Direct observation of the next leading discontinuity, i.e., the fourth derivative at $r = 3$, is a more demanding task and could not be obtained satisfactorily within the accuracy achievable for this work.

With $c_{WM}(r)$, the poles can be determined as a solutions of the pair of equations in Eqs. (3)–(4). The results for the first two poles are shown in Fig. 6 and reported in Table II. Because of the sinh and cosh functions, calculations of the higher order poles become increasingly more computationally demanding as the numerical procedure requires accurate $c(r)$ data at large separations to provide convergence of the integrals [23]. In the figure the results from the PY and PYWM approximations are also given. The PYWM approximation is like the PY approximation but in which $c_{PY}(0 < r < 1)$ is replaced by $c_{WM}(0 < r < 1)$ in Eq. (25), which allows the importance of the neglected $c(r > 1)$ PY part to be assessed. As may be seen, the results for the first pole are quite similar to those from the PY theory. Practically the same trend has been obtained recently at higher densities by directly fitting $|\ln[rh(r)]|$ to the one pole approximation for $r > 1.5$ [see Fig. 2(c) in Ref. [48]]. The inset in Fig. 6(a) shows clearly that the α value of the first pole decreases more rapidly with density than for the PY approximation and, as expected, the difference decreases at low densities. In this way some puzzling behavior obtained with less accurate $c(r)$ data in Ref. [23] may be explained. The PYWM approximation slightly improves on the PY data at intermediate densities and indicates, as seen in the inset, that for $\rho > 0.6$, the $c(r > 1)$ part has a noticeable effect on the first pole.

The $\alpha(\omega)$ dependence of the second pole [seen in Fig. 6(b)] demonstrates the importance of the $c(r > 1)$ part, which is neglected in the PY and PYWM approximations. As can be deduced from the figure, the assumption, $c(r > 1) = 0$, causes, particularly for $\rho > 0.6$, an enlargement of the period of oscillation in the RDF. This effect can be observed directly by comparing $h_{MD}(r)$ and $h_{PY}(r)$ functions.

TABLE II. The A_i, α_i, ω_i, and δ_i for the first and second poles of the HS fluid for different densities.

ρ	A_1	α_1	ω_1	δ_1	A_2	α_2	ω_2	δ_2
0.05	53.7414	5.0027	4.5098	1.0605	89.5009	6.2674	11.5108	0.6418
0.10	24.4945	4.0729	4.7607	0.9813	43.3881	5.4565	11.6245	0.5767
0.15	15.4342	3.5098	4.9570	0.9247	28.4642	4.9536	11.7228	0.5501
0.20	11.1080	3.0985	5.1229	0.8757	21.1204	4.5715	11.7983	0.5292
0.25	8.6038	2.7708	5.2704	0.8297	16.6978	4.2657	11.8551	0.5006
0.30	6.9837	2.4964	5.4104	0.7861	13.7281	3.9913	11.9174	0.4724
0.35	5.8557	2.2600	5.5409	0.7468	11.6288	3.7559	11.9910	0.4594
0.40	5.0310	2.0498	5.6659	0.7051	10.1645	3.5201	12.0497	0.4305
0.45	4.4090	1.8616	5.7876	0.6675	9.0699	3.2986	12.1266	0.3961
0.50	3.9102	1.6902	5.9062	0.6296	8.1863	3.1207	12.2074	0.3612
0.55	3.5259	1.5325	6.0234	0.5946	6.9736	2.9693	12.3056	0.3507
0.60	3.2085	1.3870	6.1384	0.5558	6.8673	2.7669	12.3905	0.2999
0.65	2.9413	1.2511	6.2530	0.5165	6.4751	2.6314	12.5060	0.2155
0.70	2.7214	1.1245	6.3672	0.4789	6.2540	2.5100	12.6630	0.1448
0.75	2.5602	1.0061	6.4812	0.4508	6.2074	2.3676	12.8220	−0.3694
0.80	2.3939	0.8943	6.5958	0.4036	4.8704	2.2718	13.0524	−0.3496
0.85	2.2652	0.7894	6.7112	0.3655	3.5655	2.1172	13.3103	−0.4879
0.88	2.1872	0.7291	6.7812	0.3463	2.6961	1.9858	13.4910	−0.4165
0.90	2.1471	0.6903	6.8290	0.3300	2.4462	1.8949	13.6030	−0.3957
0.92	2.1016	0.6524	6.8762	0.3108	2.0802	1.8180	13.6949	−0.3207
0.94	2.0719	0.6171	6.9237	0.2932	1.8606	1.7195	13.7975	−0.2774

Thus, it is the second pole and *not* the first one that mainly reflects the role of the $c(r > 1)$ region, and its subtle but important influence on the HS fluid structure. Consequently it should be taken into account in any realistic modeling of the RDF. It was checked that the HS fluid structure can be well represented to within an accuracy of 0.001 by the first two poles already at separations, $r > 1.7 + 0.8\rho$. An example of this is shown in Fig. 7 for two densities. As may be seen in the figure, the two-pole approximation reproduces well a considerable part of the $h(r;\rho)$ range.

IV. CONCLUSIONS

The SCFs of a HS fluid up to the freezing density have been investigated using a novel scheme combining accurate MD simulation data from a large system, the pole structure representation of the total correlation function $h(r)$, and the OZ equation. The important feature of the scheme is that some of the calculation stages can be performed analytically where the long range distance, r, and wave vector q contributions to the respective functions are taken into account.

It was shown with this approach how the tail of the Fourier transform of $h(r)$ contains information on the discontinuities in the derivatives of the DCF at any density. More specifically, it has been shown that $c(r)$ can be considered to be the sum of a numerically obtainable part, c_N(r), and an analytical part, $c_A(r)$, which consists of a series of relatively elementary integrals. It was found that some of the integral terms in the series are related to the sine integral special function which gives rise to the discontinuities. The order and position of the discontinuities agree with results obtained using diagrammatic techniques for the low-density expansion of the SCF. However, using the performed analysis of the higher order derivatives, no discontinuities at noninteger separations (e.g., at $r = \sqrt{3}$), were found, a feature which we think is worth studying further.

An exact, simple and closed-form formula for the jump magnitude of the discontinuities has been derived, and given in Eq. (16), which requires only the equation of state and indicates that there is a particular density, $\rho_c \cong 0.133$, below which the magnitude of the jump decreases with order of the derivative. It is not clear what aspect of the HS fluid would cause this characteristic density, ρ_c. Perhaps, one may speculate, it might be connected with the density region in which the mean field approach PY approximation starts to be a good representation of the HS liquid [as may be seen in Fig. 2 and the inset in Fig. 6(a)].

The small q-limit of the SCF is not directly accessible using the MD or MC simulation methods because of the finite-sized periodic cell used. A step forward in this respect is that $h(r)$ is expressible in terms of the pole structure, which gives a Taylor expansion about $q = 0$ of $c(q)$ that is even in q, where the expansion coefficients are functions of the pole component values. In this way the small q-region can be obtained from the pole structure. Also, the expansion coefficients can be compared with the moments of the DCF which provides a self-consistency and accuracy check of the performed calculations.

Using accurate MD simulation data the set of parameters that represents the radial distribution function in the form given in Eq. (21) have been determined. This set provides a very accurate description of the HS fluid structure. It enables us, following the calculation stages of the pole structure method, to obtain the DCF function as the sum of the $c_N(r)$ and $c_A(r)$ parts.

The DCF determined improves and adds to the existing literature data. It allows for direct observation of the discontinuity in its second derivative at $r = 2$ and demonstrates the key role of the $c_A(r)$ part in this respect. For the first time, the evaluation of the second pole of the HS fluid has become feasible, as well as the accurate calculation of the density dependence of the first pole. A comparison with the

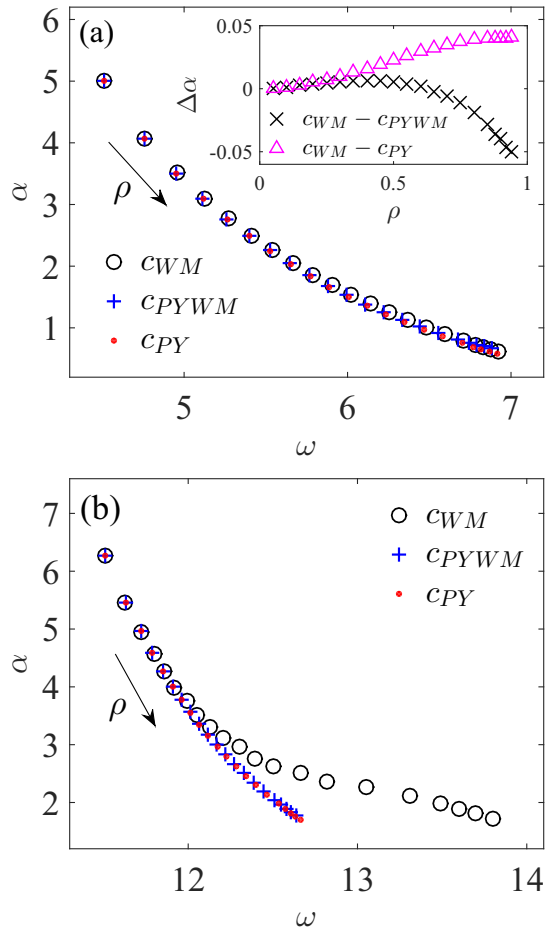

FIG. 6. The first (a) and second (b) pole of the HS fluid for several densities (see Table II) obtained from Eqs. (3)–(4) and $c_{WM}(r)$ (open circles). Dots and crosses denote the corresponding results from the PY and PYWM approximations, respectively. In the inset the deviations caused by the PY and PYWM approximations in the density dependence of α of the first pole are shown in enlarged form.

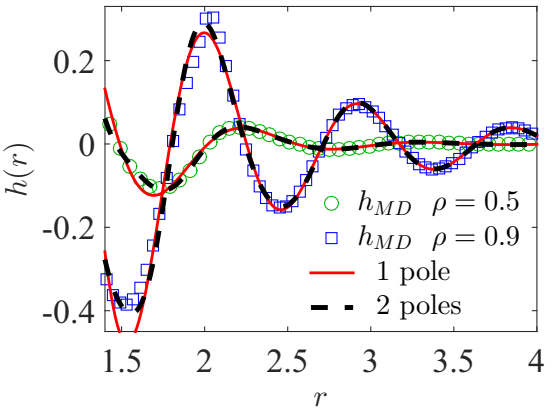

FIG. 7. The structure correlation function $h(r)$ of the HS fluid at intermediate and high densities in terms of the one and two pole approximation (the solid and dashed lines, respectively). The open symbols show the $h_{MD}(r)$ simulation data.

results obtained with the PY and PY-like approximations has demonstrated conclusively the non-negligible role of the DCF part for $r > 1$ at densities $\rho > 0.6$. With the evaluated poles the range of pair separations at each density where the two pole approximation represents well the RDF has been determined. The results obtained in this work extend our knowledge and understanding of this important HS reference fluid, which could be used in improving statistical mechanical theories of the liquid state. The proposed scheme might be applied to other model potentials with a hard core, such as Yukawa-type potentials, which are used to represent charge stabilized colloidal particles. Similarly it could be extended to square-well or square-shoulder particles [9], which are used as mean-field representations of colloidal and polymeric systems in a solvent. The analytic and numerical results of this work could be employed to develop the fundamental measure theory, perturbation, and scaled-particle statistical mechanical theories of fluids, where the HS fluid is used as a reference system [24]. Also it would be interesting to generalize the scheme to some fluid mixtures (e.g., additive HS binary mixtures). The present theory could form the basis of further developments of the pole analysis and some aspects connected with asymptotic decay of structural functions in different systems as might be seen in Ref. [48].

ACKNOWLEDGMENTS

The authors would like to thank Prof. Andrés Santos, Departamento de Física, Universidad de Extremadura, Badajoz, Spain, for useful discussions and one of the anonymous referees for pointing out Ref. [48].

APPENDIX A

In this appendix a derivation of the large q expressions in Eqs. (9)–(11) is presented. If $h(q)$ in Eq. (8) is rewritten in the form

$$h(q) = -\frac{4\pi}{q^2}\left[\frac{\sin(q)}{q} - \cos(q)\right] + \frac{2\pi}{q^2}\sum_{i=1}^{\infty} A_i e^{-\alpha_i} \times \left[\frac{\frac{\alpha_i}{q}\cos(\delta_i+\omega_i-q) - \left(\frac{\omega_i}{q}-1\right)\sin(\delta_i+\omega_i-q)}{\frac{\alpha_i^2}{q^2}+\frac{\omega_i^2}{q^2}-\frac{2\omega_i}{q}+1} - \frac{\frac{\alpha_i}{q}\cos(\delta_i+\omega_i+q) - \left(\frac{\omega_i}{q}+1\right)\sin(\delta_i+\omega_i+q)}{\frac{\alpha_i^2}{q^2}+\frac{\omega_i^2}{q^2}+\frac{2\omega_i}{q}+1}\right], \tag{A1}$$

we can exploit for large q the expansion $(1+x)^{-1} = 1 - x + x^2 - x^3 + \cdots$, and get

$$\lim_{q\to\infty} h(q) = C_1\frac{\cos(q)}{q^2} + D_1\frac{\sin(q)}{q^3} + C_2\frac{\cos(q)}{q^4} + D_2\frac{\sin(q)}{q^5} + \cdots, \tag{A2}$$

where

$$C_1 = 4\pi\left[1 + \sum_{i=1}^{\infty} A_i e^{-\alpha_i}\sin(\omega_i + \delta_i)\right], \tag{A3}$$

$$D_1 = -4\pi\left\{1 + \sum_{i=1}^{\infty} A_i e^{-\alpha_i}[\omega_i\cos(\omega_i + \delta_i) - \alpha_i\sin(\omega_i + \delta_i)]\right\}, \tag{A4}$$

$$C_2 = -4\pi\sum_{i=1}^{\infty} A_i e^{-\alpha_i}\left[\left(\alpha_i^2 - \omega_i^2\right)\sin(\omega_i + \delta_i) - 2\alpha_i\omega_i\cos(\omega_i + \delta_i)\right], \tag{A5}$$

$$D_2 = -4\pi\sum_{i=1}^{\infty} A_i e^{-\alpha_i}\left[\left(\alpha_i^3 - 3\alpha_i\omega_i^2\right)\sin(\omega_i + \delta_i) + \left(\omega_i^3 - 3\alpha_i^2\omega_i\right)\cos(\omega_i + \delta_i)\right], \tag{A6}$$

and the trigonometric relations $\sin(a \pm x) = \sin(a)\cos(x) \pm \cos(a)\sin(x)$ and $\cos(a \pm x) = \cos(a)\cos(x) \mp \sin(a)\sin(x)$ have been used. It gives the expression in Eq. (9). From the equation $Z = 2\pi\rho g(r = 1)/3$ and the pole structure representation of $h(r)$ in Eq. (7) it directly follows that $C_1 = 4\pi g(1) = 6Z/\rho$. The first few derivatives are

$$\frac{dg(r)}{dr} = \frac{1 - g(r)}{r} + \sum_{i=1}^{\infty}\frac{A_i}{r}e^{-\alpha_i r}[\omega_i\cos(\omega_i r + \delta_i) - \alpha_i\sin(\omega_i r + \delta_i)], \tag{A7}$$

$$\frac{d^2g(r)}{dr^2} = -\frac{2}{r}\frac{dg(r)}{dr} + \sum_{i=1}^{\infty}\frac{A_i}{r}e^{-\alpha_i r}\left[\left(\alpha_i^2 - \omega_i^2\right)\sin(\omega_i r + \delta_i) - 2\alpha_i\omega_i\cos(\omega_i r + \delta_i)\right], \tag{A8}$$

$$\frac{d^3g(r)}{dr^3} = -\frac{3}{r}\frac{d^2g(r)}{dr^2} - \sum_{i=1}^{\infty}\frac{A_i}{r}e^{-\alpha_i r}\left[\left(\alpha_i^3 - 3\alpha_i\omega_i^2\right) \times \sin(\omega_i r + \delta_i) + \left(\omega_i^2 - 3\alpha_i^2\omega_i\right)\cos(\omega_i r + \delta_i)\right], \tag{A9}$$

which indicates that the C_n and D_m in the expansion in Eq. (9) are related to the derivatives of the RDF at contact ($r = 1$). In particular the relations in Eqs. (10)–(11) follow directly from (A3)–(A9).

APPENDIX B

In this appendix the existence and origin of the leading discontinuities in the derivatives of the DCF is shown, and their magnitudes in Eq. (16) are derived.

The $c_A(r)$ in Eq. (13) can be considered to be composed of terms with $s = 0$, terms with $s = k$ and the remaining terms ($s \neq 0$, $s \neq k$), which we denote by $\mathbb{U}_1$, $\mathbb{U}_2$, and $\mathbb{U}_3$, respectively. The first category ($s = 0$),

$$\begin{aligned}\mathbb{U}_1 &= \frac{1}{2\pi^2 r}\sum_{k=1}^{\infty}(-\rho)^{k-1}\binom{k}{0} \times \int_Q^{\infty} dq\, q\sin(qr)\cos(q)^k\left[\sum_{n=1}^{\infty}\frac{C_n}{q^{2n}}\right]^k \\ &= \frac{1}{2\pi^2 r}\sum_{k=1}^{\infty}(-\rho)^{k-1}\sum_{n_1=1}^{\infty}\sum_{n_2=1}^{\infty}\cdots\sum_{n_k=1}^{\infty}C_{n_1}C_{n_2} \cdots C_{n_k}\int_Q^{\infty} dq\,\frac{\sin(qr)\cos(q)^k}{q^{2(n_1+n_2+\cdots+n_k)-1}},\end{aligned} \tag{B1}$$

consists of integrals

$$I_{kL} = \int_Q^{\infty} dq\,\frac{\sin(qr)\cos(q)^k}{q^{2L-1}}, \tag{B2}$$

where $k = 1,2,\ldots,$ and $L = k, k+1, k+2,\ldots$ and the lowest, $L = k$, is for the case $n_1 = n_2 = \cdots = n_k = 1$. Next, the trigonometric representation [49] of the $\sin(qr)\cos(q)^k$ can be used to express I_{kL} in terms of a sum of integrals which involve only the sine functions,

$$\begin{aligned}I_{kL}^G &= A_G\int_Q^{\infty} dq\,\frac{\sin[q(r - G)]}{q^{2L-1}} \\ &= A_G(r - G)^{2L-2}\int_{Q(r-G)}^{\infty} dx\,\frac{\sin(x)}{x^{2L-1}},\end{aligned} \tag{B3}$$

where $G = 0, \pm 1, \pm 2, \ldots, \pm k$ and A_G is a G-dependent number. For $k = 1$, also $L = 1$ and the above integral is the sine integral special function [38] $-si[Q(r - G)] = \int_{Q(r-G)}^{\infty} dx\,\sin(x)/x = \frac{\pi}{2}|\,r - G\,|/(r - G) - Si[Q(r - G)]$, where $Si(t) = \int_0^t dx\,\sin(x)/x$. This means the above integral and consequently, $c_A(r)$, has a discontinuity at $r = 1$ (because $r > 0$, and the function with $G = 0, -1$ are continuous). Note that for $L > 1$, the integral I_{kL}^G also involves the $si(x)$ function because [49]

$$\begin{aligned}\int\frac{\sin(x)}{x^{2L-1}} = \frac{(-1)^L}{x(2L-2)!}&\left[\sum_{j=0}^{L-2}(-1)^{j+1}\frac{(2j)!}{x^{2j}}\cos(x)\right. \\ &\left. + \sum_{j=0}^{L-2}(-1)^{j+1}\frac{(2j+1)!}{x^{2j+1}}\sin(x)\right] \\ &+ \frac{(-1)^{L-1}}{(2L-2)!}si(x).\end{aligned} \tag{B4}$$

Thus, for any k, the integral I_{kL}^G contains the term

$$T_{kL}^G = \frac{A_G(-1)^{L-1}}{(2L-2)!}(r - G)^{2L-2}si[Q(r - G)], \tag{B5}$$

which is a continuous function but its $(2L-2)$-th derivative has a jump at $r = G > 0$ due to the behavior of the $si(x)$ function, which goes to $\pm\pi/2$ at $r = G$. The lowest order of this derivative is for $L = k$. Also the jump in the $(2k-2)$-th derivative first occurs at $r = G = k$. For example, for the $k = 2$ term in (B5), there is a discontinuity in the second, fourth, sixth, etc., derivatives at $r = 1,2$, and for $k = 3$ there is a

discontinuity in the fourth, sixth, etc., derivatives at $r = 1,2$ and 3. Thus, at $r = 2$ the first jump occurs in the second derivative and at $r = 3$ in the fourth derivative. This means that it is the term, T^k_{kk}, in (B5) that causes the leading discontinuity in the DCF i.e., the discontinuity in the $(2k-2)$th derivative at $r = k$. In this case $A_{G=k} = 1/2^k$.

Significantly, from (B5) and taking into account all constants in expressions back to (B1), we can now obtain the jump magnitude in the leading discontinuities of the $c_A(r)$ [note for $L = k$ it is $C_{n_1} C_{n_2} \cdots C_{n_k} = (C_1)^k$],

$$\triangle_k = \left| \left[\frac{\partial^{2k-2} c_A(r)}{\partial r^{2k-2}} \right]_{r \to k^+} - \left[\frac{\partial^{2k-2} c_A(r)}{\partial r^{2k-2}} \right]_{r \to k^-} \right| = \frac{\rho^{k-1}}{k\pi 2^{k+1}} C_1^k, \tag{B6}$$

which is the result given in Eq. (16) with $C_1 = 6Z/\rho$ in Eq. (10).

The second category ($s = k$),

$$\mathbb{U}_2 = \frac{1}{2\pi^2 r} \sum_{k=1}^{\infty} (-\rho)^{k-1} \binom{k}{k} \int_Q^{\infty} dq q \sin(qr) \times \sin(q)^k \left[\sum_{m=1}^{\infty} \frac{D_m}{q^{2m+1}} \right]^k = \frac{1}{2\pi^2 r} \sum_{k=1}^{\infty} (-\rho)^{k-1} \sum_{m_1=1}^{\infty} \sum_{m_2=1}^{\infty} \cdots \sum_{m_k=1}^{\infty} D_{m_1} D_{m_2} \cdots D_{m_k} \int_Q^{\infty} dq \frac{\sin(qr)\sin(q)^k}{q^{2(m_1+m_2+\cdots+m_k)-1+k}}, \tag{B7}$$

consists of integrals of the form

$$II_{kL} = \int_Q^{\infty} dq \frac{\sin(qr)\sin(q)^k}{q^{2L-1+k}}. \tag{B8}$$

For an even index, $k = 2j$, Eq. (B8) can be transformed into (B2) using the relation $\sin(q)^{2j} = [1 - \cos(q)^2]^j$. In the denominator we have $2L + k - 1$ instead of $2L - 1$ which means that the first discontinuity of the DCF at $r = k$ occurs only in its $(3k-2)$-th derivative.

For odd $k = 2j - 1$, similar analysis to that of $\mathbb{U}_1$ leads to the integral

$$II^G_{kL} = A_G \int_Q^{\infty} dq \frac{\cos[q(r-G)]}{q^{2L+k-1}} = A_G (r-G)^{2L+k-2} \int_{Q(r-G)}^{\infty} dx \frac{\cos(x)}{x^{2L+k-1}}, \tag{B9}$$

which just as for (B3) involves the $si(x)$ function [49] and contains the term

$$TT^G_{kL} = \frac{A_G(-1)^{L-1}}{(2L+k-2)!} (r-G)^{2L+k-2} si[Q(r-G)]. \tag{B10}$$

This means that the lowest order discontinuity ($G = k$, $L = k$) of the DCF produced by the $\mathbb{U}_2$ part takes place at $r = k$ in its $(3k-2)$-th derivative.

The $\mathbb{U}_3$ case ($s \neq 0$, $s \neq k$), consists of integrals,

$$III_{kL} = \int_Q^{\infty} dq \frac{\sin(qr)\cos(q)^{k-s}\sin(q)^s}{q^{2L+s-1}}, \tag{B11}$$

where now $L = n_1 + n_2 + \cdots + n_{k-s} + m_1 + m_2 + \cdots + m_s$. If s or $k - s$ is an even number the above integral can be rearranged to the form of I_{kL} or II_{kL} with $2L + s - 1$ power in the denominator. Consequently, III_{kL} yields the first discontinuity at $r = k$ in the $\mathbb{U}_3$ part in its $2k + s - 2$ derivative. It can be shown, using the trigonometric identity $2\sin(qr)\cos(q) = \sin[q(r-1)] + \sin[q(r+1)]$, that the integrals (B11) with odd s and odd $k - s$, involve $\int_Q^{\infty} dq \sin[q(r-G)]\sin(q)^{k-1}/q^{2L+s-1}$ which yields the first discontinuity at $r = k$ also in the $(2k + s - 2)$-th derivative.

Thus, from the above considerations, the leading discontinuities in the derivatives of $c_A(r) = \mathbb{U}_1 + \mathbb{U}_2 + \mathbb{U}_3$ come from the $\mathbb{U}_1$ part or terms with $s = 0$. The leading discontinuities are at $r = k$ in the $(2k-2)$-th derivative, and their magnitude is given in (B6). Other discontinuities, generated by the integral terms in Eq. (13), occur at $r = k$ but in higher than the $(2k-2)$-th order derivatives.

APPENDIX C

In this appendix a brief summary is presented of how the scheme of Sec. II can be exploited and combined with the MD data for $h(r)$ to obtain the DCF.

By expressing the $h(r)$ in Eq. (7) by $h_{WM}(r)$ in Eq. (21) we deal with the finite number of parameters which define the function. The set of these (W+4M) parameters can be obtained by fitting the $h_{WM}(r)$ to the simulation $h_{MD}(r)$ data. In the fitting procedure the conditions in Eqs. (22)–(24) are included, and the resulting parameter values are given in the tables in Supplemental Material [46]. In this way the $h_{WM}(r)$ has been determined. Its Fourier transform can be obtained analytically,

$$\begin{aligned} h_{WM}(q) &= 4\pi \int_0^{\infty} r^2 h(r) \frac{\sin(qr)}{qr} dr \\ &= -\frac{4\pi}{q^2}\left[\frac{\sin(q)}{q} - \cos(q)\right] + \frac{2\pi}{q} \sum_{i=1}^{M} A_i e^{-\alpha_i} \left[\frac{\alpha_i \cos(\delta_i + \omega_i - q) - (\omega_i - q)\sin(\delta_i + \omega_i - q)}{\alpha_i^2 + (\omega_i - q)^2} \right. \\ &\quad \left. - \frac{\alpha_i \cos(\delta_i + \omega_i + q) - (\omega_i + q)\sin(\delta_i + \omega_i + q)}{\alpha_i^2 + (\omega_i + q)^2} \right] + 4\pi \left[\sum_{n=1}^{8} (-1)^{n-1} \frac{ST_n}{q^{2n}} \cos(q) \right. \\ &\quad \left. - \sum_{n=1}^{8} (-1)^{n-1} \frac{ST_{8+n}}{q^{2n+1}} \sin(q) - \sum_{n=1}^{8} (-1)^{n-1} \frac{ST_{16+n}}{q^{2n}} \cos(qR) + \sum_{n=1}^{8} (-1)^{n-1} \frac{ST_{24+n}}{q^{2n+1}} \sin(qR) \right], \end{aligned} \tag{C1}$$

where $ST_n = \sum_{j=1}^{15} a_j^{(n)} b_j^{(n)}$, and the coefficients $a_j^{(n)}$ are taken from tables in Supplemental Material [46] for different densities.

Following Sec. II, the large q-limit ($q > Q$) of the $h_{WM}(q)$ is calculated:

$$h_{WM}^{\text{tail}}(q) = \cos(q)\left[\sum_{n=1} \frac{C_{n1}}{q^{2n}}\right] + \cos(qR)\left[\sum_{n=1} \frac{C_{n2}}{q^{2n}}\right] + \sin(q)\left[\sum_{m=1} \frac{D_{m1}}{q^{2m+1}}\right] + \sin(qR)\left[\sum_{m=1} \frac{D_{m2}}{q^{2m+1}}\right]. \tag{C2}$$

It was verified that the series converges quickly and it is sufficient to consider terms up to q^{-5}. The coefficients in the above expansion are

$$C_{11} = 4\pi[1 + ST_1], \tag{C3}$$

$$C_{12} = 4\pi\left[\sum_{i=1}^{M} A_i e^{-\alpha_i R} \sin(\omega_i R + \delta_i) - ST_{17}\right], \tag{C4}$$

$$D_{11} = -4\pi[1 + ST_9], \tag{C5}$$

$$D_{12} = -4\pi\left\{\sum_{i=1}^{M} A_i e^{-\alpha_i R}[\omega_i \cos(\omega_i R + \delta_i) - \alpha_i \sin(\omega_i R + \delta_i)] - ST_{25}\right\}, \tag{C6}$$

$$C_{21} = -4\pi ST_2, \tag{C7}$$

$$C_{22} = -4\pi\left\{\sum_{i=1}^{M} A_i e^{-\alpha_i R}\left[\left(\alpha_i^2 - \omega_i^2\right)\sin(\omega_i R + \delta_i) - 2\alpha_i\omega_i \cos(\omega_i R + \delta_i)\right] - ST_{18}\right\}, \tag{C8}$$

$$D_{21} = 4\pi ST_{10}, \tag{C9}$$

$$D_{22} = -4\pi\left\{\sum_{i=1}^{M} A_i e^{-\alpha_i R}\left[\left(\alpha_i^3 - 3\alpha_i\omega_i^2\right)\sin(\omega_i R + \delta_i) + \left(\omega_i^3 - 3\alpha_i^2\omega_i\right)\cos(\omega_i R + \delta_i)\right] + ST_{26}\right\}. \tag{C10}$$

Thus, Eqs. (C1) and (C2), along with tables in Supplemental Material [46] give $h_{WM}(q)$ and $h_{WM}^{\text{tail}}(q)$.

Then, as in Sec. II, the DCF function is considered to be the sum of two parts: $c_{WM}(r) = c_{WM}^{N}(r) + c_{WM}^{A}(r)$. The first is obtained numerically,

$$c_{WM}^{N}(r) = \frac{1}{2\pi^2}\int_0^Q q^2 \frac{h_{WM}(q)}{1 + \rho h_{WM}(q)} \frac{\sin(qr)}{qr}\, dq, \tag{C11}$$

with $h_{WM}(q)$ from Eq. (C1), and the second is analytic,

$$\begin{aligned} c_{WM}^{A}(r) &= \frac{1}{2\pi^2}\int_Q^\infty q^2 \frac{h_{WM}^{\text{tail}}(q)}{1 + \rho h_{WM}^{\text{tail}}(q)} \frac{\sin(qr)}{qr}\, dq \\ &= \int_Q^\infty \frac{[C_{11}\cos(q) + C_{12}\cos(qR)]\sin(qr)}{2\pi^2 qr}\, dq + \int_Q^\infty \frac{[D_{11}\sin(q) + D_{12}\sin(qR)]\sin(qr)}{2\pi^2 q^2 r}\, dq \\ &\quad + \int_Q^\infty \frac{[C_{21}\cos(q) + C_{22}\cos(qR)]\sin(qr)}{2\pi^2 q^3 r}\, dq - \int_Q^\infty \frac{\rho[C_{11}\cos(q) + C_{12}\cos(qR)]^2 \sin(qr)}{2\pi^2 q^3 r}\, dq \\ &\quad + \int_Q^\infty \frac{[D_{21}\sin(q) + D_{22}\sin(qR)]\sin(qr)}{2\pi^2 q^4 r}\, dq \\ &\quad - \int_Q^\infty \frac{2\rho[C_{11}\cos(q) + C_{12}\cos(qR)][D_{11}\sin(q) + D_{12}\sin(qR)]\sin(qr)}{2\pi^2 q^4 r} dq + \cdots, \end{aligned} \tag{C12}$$

where only a few lowest order terms are written out. In calculations, depending on density, the Q value was from 100 to 200. It was checked that $C_{n1} \gg C_{n2}$, $D_{m1} \gg D_{m2}$ and all terms with the (qR) argument are negligible, which means the above expression is practically the same as $c_A(r)$ in Eq. (13). Equations (C11) and (C12) were used, along with the coefficients in tables in Supplemental Material [46]. The results of these steps are given in tables in Appendix D and in the figures in the main text.

APPENDIX D

In this Appendix tables with the obtained DCF are presented. The results at the various densities according to the scheme presented in Sec. II and Appendix C for $0 < r < 1$ are given in Table III and for $r > 1$ are given in Tables IV and V.

TABLE III. Coefficients for $c(0 < r < 1; \rho)$ in Eq. (25).

ρ	λ_1	λ_2	λ_3	λ_4	λ_5	λ_6	λ_7	λ_8	λ_9	λ_{10}	λ_{11}
0.05	−0.0064436392	0.033141627	−0.073020345	0.089684305	−0.0669075	0.030980218	−0.008825822	−0.014424959	−0.00044896945	0.1794399	−1.2314384
0.10	−1.1403294	6.1146344	−14.122845	18.381365	−14.808024	7.6358321	−2.5192459	0.47809973	−0.063852407	0.41518482	−1.5133492
0.15	−0.50356898	2.6950268	−6.2196811	8.1008828	−6.5424588	3.3892937	−1.1296743	0.17053684	−0.039698319	0.7128001	−1.8568049
0.20	−1.5972292	8.5625916	−19.778566	25.75009	−20.749498	10.702038	−3.5462652	0.64118595	−0.12225528	1.1025637	−2.2760142
0.25	−0.25013904	1.3013604	−2.9206636	3.6902558	−2.8669445	1.416893	−0.48878196	0.002848882	−0.10020279	1.5961781	−2.7880606
0.30	−0.31800916	1.6642616	−3.7802565	4.8693678	−3.8903496	2.0153492	−0.78476732	0.10139401	−0.21314878	2.2391453	−3.4149933
0.35	0.11502209	−0.63115109	1.4441218	−1.8295411	1.4506754	−0.69288014	−0.040277628	0.060576699	−0.387316	3.0684085	−4.1838655
0.40	0.98243283	−5.2299612	11.892435	−15.173902	12.01117	−5.9659401	1.3570567	0.061529863	−0.70001265	4.1431401	−5.1294155
0.45	−1.7943547	9.805173	−23.284825	31.271958	−25.942754	14.068444	−5.9585997	2.160661	−1.4718303	5.5531542	−6.2957397
0.50	−2.6256831	14.286222	−33.879785	45.524523	−37.89612	20.973193	−9.5950509	4.0961401	−2.5714253	7.3871964	−7.739026
0.55	−3.9679551	21.748135	−52.128782	70.961414	−60.102559	34.412181	−16.771562	7.8022395	−4.4256464	9.7981081	−9.5319257
0.60	−9.1032588	50.058988	−120.24275	164.20408	−140.09145	80.633011	−37.544481	16.16339	−7.6966883	12.998175	−11.76921
0.65	−14.221544	78.431398	−189.6337	261.63403	−226.98451	134.81788	−65.605709	29.162643	−12.870737	17.251037	−14.575458
0.70	6.4268617	−28.754556	46.089964	−24.851989	−18.90467	49.440092	−57.386698	40.302333	−19.947651	22.877442	−18.114034
0.75	−20.130131	121.64271	−328.05635	508.85777	−501.57075	346.14662	−193.66235	90.617488	−34.994893	30.683634	−22.613264
0.80	56.139841	−261.4202	479.15739	−415.06406	108.98833	139.68257	−200.73052	131.31962	−54.142772	41.060545	−28.355862
0.85	137.36003	−640.4304	1188.8622	−1071.6175	361.01321	223.80897	−365.34487	231.0741	−88.146522	55.50192	−35.770092
0.88	190.94356	−858.38161	1494.7479	−1158.1925	116.68779	579.88859	−618.12858	343.16899	−120.26791	66.884539	−41.251793
0.90	175.79911	−719.5333	1011.5289	−276.79011	−843.41445	1255.9387	−947.60094	458.34318	−148.75615	75.880035	−45.45262
0.92	314.52457	−1364.1004	2221.3318	−1415.2089	−359.42592	1310.3087	−1130.0437	562.56337	−180.20162	86.152768	−50.114574
0.94	458.68514	−1991.9413	3270.3201	−2163.2789	−356.55347	1715.3319	−1473.416	714.45833	−220.73566	98.089592	−55.343664

TABLE IV. The DCF at the various densities according to the scheme presented in Sec. II and Appendix C.

	DCF at density										
r	0.05	0.10	0.15	0.20	0.25	0.30	0.35	0.40	0.45	0.50	0.55
1.00	0.0005	0.0021	0.0052	0.0103	0.0180	0.0290	0.0444	0.0648	0.0920	0.1273	0.1730
1.02	0.0004	0.0018	0.0045	0.0089	0.0155	0.0246	0.0373	0.0539	0.0755	0.1029	0.1375
1.04	0.0004	0.0016	0.0039	0.0077	0.0132	0.0208	0.0311	0.0444	0.0612	0.0821	0.1076
1.06	0.0004	0.0014	0.0034	0.0066	0.0112	0.0174	0.0258	0.0362	0.0491	0.0645	0.0828
1.08	0.0003	0.0012	0.0029	0.0056	0.0094	0.0144	0.0211	0.0291	0.0388	0.0497	0.0622
1.10	0.0003	0.0010	0.0025	0.0047	0.0079	0.0118	0.0171	0.0231	0.0301	0.0375	0.0453
1.12	0.0003	0.0009	0.0021	0.0039	0.0065	0.0096	0.0136	0.0180	0.0228	0.0274	0.0317
1.14	0.0002	0.0008	0.0018	0.0033	0.0053	0.0077	0.0107	0.0137	0.0168	0.0192	0.0209
1.16	0.0002	0.0006	0.0015	0.0027	0.0043	0.0060	0.0082	0.0101	0.0118	0.0127	0.0124
1.18	0.0002	0.0005	0.0013	0.0022	0.0034	0.0046	0.0061	0.0072	0.0079	0.0075	0.0059
1.20	0.0001	0.0005	0.0010	0.0018	0.0026	0.0035	0.0044	0.0048	0.0047	0.0035	0.0011
1.22	0.0001	0.0004	0.0009	0.0014	0.0020	0.0025	0.0030	0.0029	0.0023	0.0006	−0.0023
1.24	0.0001	0.0003	0.0007	0.0011	0.0015	0.0017	0.0019	0.0014	0.0005	−0.0015	−0.0045
1.26	0.0001	0.0003	0.0005	0.0008	0.0011	0.0011	0.0010	0.0003	−0.0008	−0.0029	−0.0058
1.28	0.0001	0.0002	0.0004	0.0006	0.0007	0.0006	0.0004	−0.0005	−0.0017	−0.0037	−0.0064
1.30	0.0001	0.0002	0.0003	0.0004	0.0004	0.0002	−0.0001	−0.0010	−0.0023	−0.0041	−0.0064
1.32	0.0001	0.0001	0.0002	0.0005	0.0002	−0.0001	−0.0005	−0.0014	−0.0025	−0.0041	−0.0060
1.34	0.0001	0.0001	0.0001	0.0003	0.0001	−0.0003	−0.0007	−0.0015	−0.0025	−0.0039	−0.0053
1.36	0.0000	0.0001	0.0001	0.0003	0.0000	−0.0004	−0.0008	−0.0016	−0.0024	−0.0034	−0.0044
1.38	-	0.0000	0.0001	0.0002	−0.0001	−0.0005	−0.0008	−0.0015	−0.0021	−0.0029	−0.0033
1.40	-	-	0.0000	0.0002	−0.0002	−0.0006	−0.0008	−0.0014	−0.0018	−0.0022	−0.0023
1.42	-	-	-	0.0001	−0.0002	−0.0005	−0.0007	−0.0012	−0.0014	−0.0016	−0.0013
1.44	-	-	-	0.0000	−0.0002	−0.0005	−0.0006	−0.0009	−0.0010	−0.0009	−0.0003
1.46	-	-	-	-	−0.0002	−0.0005	−0.0005	−0.0007	−0.0006	−0.0003	0.0005
1.48	-	-	-	-	−0.0002	−0.0004	−0.0004	−0.0004	−0.0002	0.0002	0.0011
1.50	-	-	-	-	−0.0001	−0.0003	−0.0002	−0.0002	0.0001	0.0006	0.0017
1.52	-	-	-	-	0.0000	−0.0002	−0.0001	0.0000	0.0004	0.0010	0.0020
1.54	-	-	-	-	-	−0.0002	0.0000	0.0002	0.0006	0.0012	0.0022
1.56	-	-	-	-	-	−0.0001	0.0001	0.0003	0.0007	0.0013	0.0022

TABLE IV. (*Continued*.)

	DCF at density										
r	0.05	0.10	0.15	0.20	0.25	0.30	0.35	0.40	0.45	0.50	0.55
1.58	-	-	-	-	-	−0.0001	0.0002	0.0004	0.0008	0.0014	0.0021
1.60	-	-	-	-	-	0.0000	0.0003	0.0004	0.0008	0.0013	0.0019
1.62	-	-	-	-	-	-	0.0003	0.0005	0.0008	0.0012	0.0015
1.64	-	-	-	-	-	-	0.0003	0.0004	0.0007	0.0010	0.0011
1.66	-	-	-	-	-	-	0.0002	0.0004	0.0006	0.0007	0.0007
1.68	-	-	-	-	-	-	0.0001	0.0003	0.0005	0.0005	0.0002
1.70	-	-	-	-	-	-	0.0000	0.0003	0.0004	0.0002	−0.0002
1.72	-	-	-	-	-	-	-	0.0002	0.0002	0.0000	−0.0006
1.74	-	-	-	-	-	-	-	0.0001	0.0001	−0.0003	−0.0009
1.76	-	-	-	-	-	-	-	0.0001	0.0000	−0.0004	−0.0011
1.78	-	-	-	-	-	-	-	0.0000	−0.0001	−0.0005	−0.0012
1.80	-	-	-	-	-	-	-	0.0000	−0.0002	−0.0006	−0.0012
1.82	-	-	-	-	-	-	-	-	−0.0002	−0.0006	−0.0011
1.84	-	-	-	-	-	-	-	-	−0.0002	−0.0006	−0.0009
1.86	-	-	-	-	-	-	-	-	−0.0001	−0.0005	−0.0007
1.88	-	-	-	-	-	-	-	-	0.0000	−0.0004	−0.0005
1.90	-	-	-	-	-	-	-	-	-	−0.0003	−0.0003
1.92	-	-	-	-	-	-	-	-	-	−0.0001	−0.0001
1.94	-	-	-	-	-	-	-	-	-	0.0000	0.0001
1.96	-	-	-	-	-	-	-	-	-	0.0000	0.0002
1.98	-	-	-	-	-	-	-	-	-	0.0001	0.0003
2.00	-	-	-	-	-	-	-	-	-	0.0001	0.0002

TABLE V. The DCF at the various densities according to the scheme presented in Sec. II and Appendix C.

	DCF at density									
r	0.60	0.65	0.70	0.75	0.80	0.85	0.88	0.90	0.92	0.94
1.00	0.232	0.307	0.401	0.521	0.676	0.872	1.018	1.122	1.247	1.381
1.02	0.181	0.235	0.300	0.379	0.478	0.597	0.683	0.740	0.811	0.883
1.04	0.139	0.176	0.219	0.268	0.326	0.391	0.437	0.462	0.498	0.530
1.06	0.104	0.128	0.154	0.181	0.211	0.239	0.258	0.265	0.278	0.285
1.08	0.076	0.090	0.104	0.115	0.125	0.130	0.132	0.128	0.128	0.121
1.10	0.053	0.060	0.065	0.065	0.063	0.054	0.047	0.037	0.030	0.016
1.12	0.035	0.037	0.036	0.030	0.020	0.003	−0.008	−0.020	−0.030	−0.047
1.14	0.021	0.019	0.014	0.004	−0.009	−0.028	−0.040	−0.052	−0.063	−0.078
1.16	0.011	0.007	−0.001	−0.012	−0.026	−0.045	−0.056	−0.067	−0.075	−0.088
1.18	0.003	−0.002	−0.011	−0.022	−0.035	−0.051	−0.060	−0.069	−0.075	−0.084
1.20	−0.003	−0.008	−0.016	−0.027	−0.038	−0.051	−0.056	−0.062	−0.065	−0.071
1.22	−0.006	−0.012	−0.019	−0.028	−0.036	−0.045	−0.047	−0.050	−0.050	−0.053
1.24	−0.008	−0.013	−0.020	−0.026	−0.032	−0.036	−0.035	−0.036	−0.033	−0.033
1.26	−0.009	−0.014	−0.018	−0.023	−0.026	−0.026	−0.022	−0.020	−0.015	−0.013
1.28	−0.009	−0.013	−0.016	−0.018	−0.018	−0.015	−0.009	−0.005	0.002	0.005
1.30	−0.009	−0.011	−0.013	−0.013	−0.011	−0.005	0.003	0.009	0.016	0.021
1.32	−0.008	−0.009	−0.009	−0.008	−0.003	0.005	0.014	0.020	0.027	0.033
1.34	−0.006	−0.006	−0.006	−0.003	0.003	0.013	0.023	0.029	0.036	0.042
1.36	−0.005	−0.004	−0.002	0.002	0.009	0.019	0.029	0.035	0.041	0.047
1.38	−0.003	−0.002	0.001	0.006	0.013	0.023	0.033	0.039	0.044	0.048
1.40	−0.001	0.000	0.004	0.009	0.017	0.026	0.034	0.039	0.044	0.047
1.42	0.000	0.002	0.006	0.012	0.018	0.027	0.034	0.038	0.042	0.043
1.44	0.001	0.004	0.007	0.013	0.019	0.026	0.032	0.035	0.037	0.037
1.46	0.002	0.005	0.009	0.014	0.018	0.024	0.028	0.030	0.031	0.030
1.48	0.003	0.006	0.009	0.014	0.017	0.020	0.022	0.023	0.023	0.020
1.50	0.004	0.006	0.009	0.013	0.014	0.015	0.017	0.016	0.013	0.009
1.52	0.004	0.006	0.008	0.011	0.011	0.011	0.010	0.008	0.003	−0.005
1.54	0.004	0.006	0.007	0.009	0.008	0.004	0.002	−0.002	−0.008	−0.017

TABLE V. (*Continued*.)

	DCF at density									
r	0.60	0.65	0.70	0.75	0.80	0.85	0.88	0.90	0.92	0.94
1.56	0.004	0.005	0.006	0.007	0.004	−0.002	−0.007	−0.011	−0.018	−0.028
1.58	0.003	0.004	0.004	0.005	0.000	−0.008	−0.014	−0.019	−0.028	−0.039
1.60	0.003	0.003	0.002	0.002	−0.005	−0.014	−0.021	−0.026	−0.036	−0.047
1.62	0.002	0.002	0.001	−0.001	−0.008	−0.019	−0.026	−0.032	−0.041	−0.053
1.64	0.001	0.001	−0.001	−0.004	−0.012	−0.023	−0.030	−0.036	−0.045	−0.056
1.66	0.000	−0.001	−0.003	−0.006	−0.014	−0.025	−0.032	−0.037	−0.046	−0.056
1.68	0.000	−0.002	−0.004	−0.008	−0.016	−0.025	−0.032	−0.036	−0.043	−0.051
1.70	−0.001	−0.003	−0.006	−0.009	−0.016	−0.024	−0.029	−0.032	−0.037	−0.043
1.72	−0.002	−0.003	−0.006	−0.009	−0.015	−0.021	−0.023	−0.024	−0.027	−0.030
1.74	−0.002	−0.004	−0.006	−0.008	−0.013	−0.016	−0.015	−0.014	−0.014	−0.014
1.76	−0.002	−0.004	−0.006	−0.006	−0.009	−0.009	−0.006	−0.002	0.000	0.004
1.78	−0.002	−0.003	−0.005	−0.004	−0.005	−0.002	0.004	0.010	0.015	0.021
1.80	−0.002	−0.003	−0.003	−0.002	−0.001	0.005	0.013	0.020	0.027	0.035
1.82	−0.002	−0.002	−0.002	0.001	0.003	0.011	0.020	0.028	0.036	0.044
1.84	−0.001	−0.001	−0.001	0.003	0.007	0.016	0.025	0.033	0.040	0.048
1.86	−0.001	0.000	0.001	0.005	0.009	0.018	0.027	0.034	0.040	0.046
1.88	0.000	0.000	0.002	0.006	0.010	0.019	0.026	0.031	0.035	0.038
1.90	0.000	0.001	0.003	0.007	0.011	0.017	0.022	0.025	0.026	0.025
1.92	0.000	0.001	0.003	0.007	0.010	0.014	0.016	0.017	0.015	0.010
1.94	0.001	0.002	0.003	0.007	0.008	0.009	0.008	0.007	0.002	−0.006
1.96	0.001	0.002	0.003	0.005	0.005	0.003	0.000	−0.004	−0.011	−0.022
1.98	0.001	0.001	0.002	0.004	0.003	−0.002	−0.007	−0.012	−0.021	−0.033
2.00	0.001	0.001	0.002	0.003	0.000	−0.006	−0.012	−0.018	−0.027	−0.039
2.02	0.000	0.001	0.001	0.002	−0.002	−0.009	−0.015	−0.020	−0.029	−0.040
2.04	-	0.001	0.000	0.001	−0.003	−0.010	−0.015	−0.020	−0.028	−0.036
2.06	-	0.000	0.000	0.000	−0.004	−0.010	−0.015	−0.019	−0.025	−0.032
2.08	-	0.000	−0.001	−0.001	−0.005	−0.010	−0.014	−0.017	−0.022	−0.026
2.10	-	0.000	−0.001	−0.001	−0.005	−0.009	−0.012	−0.014	−0.017	−0.020
2.12	-	0.000	−0.001	−0.001	−0.005	−0.008	−0.010	−0.011	−0.013	−0.015
2.14	-	0.000	−0.001	−0.002	−0.004	−0.007	−0.008	−0.008	−0.009	−0.009
2.16	-	−0.001	−0.001	−0.001	−0.004	−0.005	−0.005	−0.005	−0.005	−0.004
2.18	-	−0.001	−0.001	−0.001	−0.003	−0.003	−0.003	−0.002	−0.001	0.000
2.20	-	−0.001	−0.001	−0.001	−0.002	−0.002	−0.001	0.001	0.002	0.004
2.22	-	−0.001	−0.001	−0.001	−0.002	0.000	0.001	0.003	0.004	0.006
2.24	-	−0.001	−0.001	0.000	−0.001	0.001	0.003	0.005	0.006	0.008
2.26	-	−0.001	−0.001	0.000	0.000	0.002	0.004	0.006	0.007	0.009
2.28	-	0.000	−0.001	0.000	0.001	0.003	0.005	0.007	0.008	0.010
2.30	-	-	0.000	0.001	0.001	0.004	0.005	0.007	0.008	0.009
2.32	-	-	-	0.001	0.002	0.004	0.006	0.007	0.008	0.008
2.34	-	-	-	0.001	0.002	0.004	0.005	0.007	0.006	0.006
2.36	-	-	-	0.001	0.002	0.004	0.005	0.006	0.005	0.005
2.38	-	-	-	0.001	0.002	0.004	0.004	0.004	0.003	0.002
2.40	-	-	-	0.001	0.002	0.003	0.003	0.003	0.002	0.000
2.42	-	-	-	0.001	0.002	0.002	0.002	0.002	0.000	−0.002
2.44	-	-	-	0.001	0.002	0.002	0.001	0.000	−0.002	−0.005
2.46	-	-	-	0.001	0.001	0.001	0.000	−0.001	−0.004	−0.007
2.48	-	-	-	0.001	0.001	0.000	−0.002	−0.003	−0.005	−0.008
2.50	-	-	-	0.001	0.000	0.000	−0.003	−0.004	−0.007	−0.009
2.52	-	-	-	0.000	0.000	−0.001	−0.003	−0.005	−0.007	−0.010
2.54	-	-	-	0.000	0.000	−0.002	−0.004	−0.005	−0.008	−0.010
2.56	-	-	-	0.000	−0.001	−0.002	−0.004	−0.005	−0.007	−0.009
2.58	-	-	-	0.000	−0.001	−0.002	−0.004	−0.005	−0.007	−0.008
2.60	-	-	-	0.000	−0.001	−0.002	−0.004	−0.005	−0.006	−0.007
2.62	-	-	-	−0.001	−0.001	−0.002	−0.004	−0.004	−0.005	−0.005
2.64	-	-	-	−0.001	−0.001	−0.002	−0.003	−0.003	−0.003	−0.003
2.66	-	-	-	−0.001	−0.001	−0.002	−0.002	−0.002	−0.001	0.000
2.68	-	-	-	−0.001	−0.001	−0.001	−0.001	−0.001	0.000	0.001

TABLE V. (*Continued*.)

	DCF at density									
r	0.60	0.65	0.70	0.75	0.80	0.85	0.88	0.90	0.92	0.94
2.70	-	-	-	−0.001	−0.001	0.000	0.000	0.001	0.002	0.003
2.72	-	-	-	−0.001	−0.001	0.000	0.001	0.002	0.003	0.005
2.74	-	-	-	−0.001	0.000	0.001	0.001	0.003	0.004	0.006
2.76	-	-	-	0.000	0.000	0.001	0.002	0.003	0.005	0.006
2.78	-	-	-	-	0.000	0.002	0.003	0.004	0.005	0.006
2.80	-	-	-	-	0.001	0.002	0.003	0.004	0.005	0.006
2.82	-	-	-	-	0.001	0.002	0.003	0.004	0.004	0.005
2.84	-	-	-	-	0.001	0.002	0.002	0.003	0.003	0.003
2.86	-	-	-	-	0.001	0.002	0.002	0.002	0.002	0.002
2.88	-	-	-	-	0.001	0.002	0.001	0.002	0.001	0.000
2.90	-	-	-	-	0.001	0.001	0.001	0.001	0.000	−0.001
2.92	-	-	-	-	0.001	0.001	0.000	0.000	−0.001	−0.002
2.94	-	-	-	-	0.001	0.001	−0.001	−0.001	−0.002	−0.003
2.96	-	-	-	-	0.000	0.000	−0.001	−0.002	−0.003	−0.004
2.98	-	-	-	-	-	-	−0.001	−0.002	−0.003	−0.005
3.00	-	-	-	-	-	-	0.000	−0.001	−0.002	−0.004

[1] N. H. March and M. P. Tosi, *Atomic Dynamics in Liquids* (Macmillan, London, 1976).
[2] D. M. Heyes, *The Liquid State* (Wiley, Chichester, 1998).
[3] P. A. Egelstaff, *An Introduction to the Liquid State*, 2nd ed. (Clarendon Press, Oxford, 1992).
[4] V. Van Hoang and N. H. Cuong, Physica B: Condensed Matter **404**, 340 (2009).
[5] V. Van Hoang and T. Odagaki, Phys. Rev. B **77**, 125434 (2008).
[6] S. V. Sukhomlinov and M. H. Müser, J. Chem. Phys. **146**, 024506 (2017).
[7] J. P. Hansen and I. R. McDonald, *Theory of Simple Liquids*, 3rd. ed. (Academic Press, New York, 2005).
[8] D. M. Heyes and A. Santos, J. Chem. Phys. **145**, 214504 (2016).
[9] A. Santos, *A Concise Course on the Theory of Classical Liquids* (Springer, Berlin, 2016).
[10] J. K. Percus and G. J. Yevick, Phys. Rev. **110**, 1 (1958).
[11] M. S. Wertheim, Phys. Rev. Lett. **10**, 321 (1963).
[12] M. S. Wertheim, J. Math. Phys. **5**, 643 (1964).
[13] E. J. Thiele, J. Chem. Phys. **38**, 1959 (1963).
[14] C. F. Tejero, and M. López de Haro, Mol. Phys. **105**, 2999 (2007).
[15] S. B. Yuste and A. Santos, Phys. Rev. A **43**, 5418 (1991).
[16] M. López de Haro, S. B. Yuste, and A. Santos, in *Theory and Simulation of Hard-Sphere Fluids and Related Systems*, edited by A. Mulero, Lecture Notes in Physics Vol. 753 (Springer, Berlin, 2008), pp. 183–245.
[17] T. Fukudome, D. Mitarai, and M. Irisa, J. Mol. Liq. **200**, 95 (2014).
[18] Y. Rosenfeld, Phys. Rev. Lett. **63**, 980 (1989).
[19] H. Hansen-Goos and R. Roth, J. Phys.: Condens. Matter **18**, 8413 (2006).
[20] H. Hansen-Goos, M. Mortazavifar, M. Oettel, and R. Roth, Phys. Rev. E **91**, 052121 (2015).
[21] R. D. Groot, J. P. van der Eerden, and N. M. Faber, J. Chem. Phys **87**, 2263 (1987).
[22] A. González and J. A. White, Physica A **296**, 347 (2001).
[23] M. Dijkstra and R. Evans, J. Chem. Phys. **112**, 1449 (2000).
[24] J. P. Hansen and I. R. McDonald, *Theory of Simple Liquids: With Applications of Soft Matter*, 4th ed. (Academic Press, New York, 2013).
[25] R. Evans, R. J. F. Leote de Carvalho, J. R. Henderson, and D. C. Hoyle, J. Chem. Phys. **100**, 591 (1994).
[26] R. Evans, J. R. Henderson, D. C. Hoyle, A. O. Parry, and Z. A. Sabeur, Mol. Phys. **80**, 755 (1993).
[27] R. J. F. Leote de Carvalho, R. Evans, D. C. Hoyle, and J. R. Henderson, J. Phys.: Condens. Matter **6**, 9275 (1994).
[28] M. E. Fisher and B. Widom, J. Chem. Phys. **50**, 3756 (1969).
[29] P. Hopkins, A. J. Archer, and R. Evans, Phys. Rev. E **71**, 027401 (2005).
[30] R. J. F. Leote de Carvalho, R. Evans, and Y. Rosenfeld, Phys. Rev. E **59**, 1435 (1999).
[31] A. C. Brańka and D. M. Heyes, J. Chem. Phys. **134**, 064115 (2011).
[32] T. Aslyamov, arXiv:1610.02812 [cond-mat.stat-mech].
[33] J. W. Perram and E. R. Smith, J. Phys. A: Math. Gen. **13**, 2219 (1980).
[34] C. Grodon, M. Dijkstra, R. Evans, and R. Roth, J. Chem. Phys. **121**, 7869 (2004).
[35] J. Kolafa, S. Labík, and A. Malijevský, Mol. Phys. **100**, 2629 (2002).
[36] M. Francová, A. Malijevský, S. Labík, and J. Kolafa, Collect. Czech. Chem. Commun. **76**, 51 (2011).
[37] J. Kolafa and S. Labík, Mol. Phys. **104**, 1915 (2006).
[38] F. W. J. Olver, D. W. Lozier, R. F. Boisvert, and C. W. Clark, *NIST Handbook of Mathematical Functions* (Cambridge University Press, Cambridge, 2010).
[39] J. Kolafa, S. Labík, and A. Malijevský, Phys. Chem. Chem. Phys. **6**, 2335 (2004).
[40] A. Trokhymchuk, I. Nezbeda, J. Jirsák, and D. Henderson, J. Chem. Phys. **123**, 024501 (2005).

[41] A. Malijevský, J. Kolafa, in *Theory and Simulation of Hard-Sphere Fluids and Related Systems*, edited by A. Mulero, Lecture Notes in Physics Vol. 753 (Springer, Berlin, 2008), p. 1.
[42] J. M. Haile, *Molecular Dynamics Simulation: Elementary Methods* (Wiley, New York, 1992).
[43] M. P. Allen and D. J. Tildesley, *Computer Simulation of Liquids* (Oxford University Press, New York, 1989).
[44] J. J. Salacuse, A. R. Denton, and P. A. Egelstaff, Phys Rev. E **53**, 2382 (1996).
[45] A. Baumketner and Y. Hiwatari, Phys. Rev. E **63**, 061201 (2001).
[46] See Supplemental Material at http://link.aps.org/supplemental/10.1103/PhysRevE.95.062104 for additional information.
[47] http://old.vscht.cz/fch/software/hsmd/.
[48] A. Statt, R. Pinchaipat, F. Turci, R. Evans, and C. P. Royall, J. Chem. Phys. **144**, 144506 (2016).
[49] I. S. Gradshteyn and I. M. Ryzhik, *Table of Integrals, Series, and Products*, 5th ed. (Academic Press, New York, 1994).